

# OpenSTL: A Comprehensive Benchmark of Spatio-Temporal Predictive Learning

Cheng Tan<sup>1,2\*</sup>, Siyuan Li<sup>1,2\*</sup>, Zhangyang Gao<sup>1,2</sup>, Wenfei Guan<sup>3</sup>,  
Zedong Wang<sup>2</sup>, Zicheng Liu<sup>1,2</sup>, Lirong Wu<sup>1,2</sup>, and Stan Z. Li<sup>2†</sup>

<sup>1</sup>Zhejiang University, <sup>3</sup>Xidian University

<sup>2</sup>AI Lab, Research Center for Industries of the Future, Westlake University

## Abstract

Spatio-temporal predictive learning is a learning paradigm that enables models to learn spatial and temporal patterns by predicting future frames from given past frames in an unsupervised manner. Despite remarkable progress in recent years, a lack of systematic understanding persists due to the diverse settings, complex implementation, and difficult reproducibility. Without standardization, comparisons can be unfair and insights inconclusive. To address this dilemma, we propose OpenSTL, a comprehensive benchmark for spatio-temporal predictive learning that categorizes prevalent approaches into recurrent-based and recurrent-free models. OpenSTL provides a modular and extensible framework implementing various state-of-the-art methods. We conduct standard evaluations on datasets across various domains, including synthetic moving object trajectory, human motion, driving scenes, traffic flow and weather forecasting. Based on our observations, we provide a detailed analysis of how model architecture and dataset properties affect spatio-temporal predictive learning performance. Surprisingly, we find that recurrent-free models achieve a good balance between efficiency and performance than recurrent models. Thus, we further extend the common MetaFormers to boost recurrent-free spatial-temporal predictive learning. We open-source the code and models at [github.com/chengtang9907/OpenSTL](https://github.com/chengtang9907/OpenSTL).

## 1 Introduction

Recent years have witnessed rapid and remarkable progress in spatio-temporal predictive learning [34, 26, 9, 37]. This burgeoning field aims to learn latent spatial and temporal patterns through the challenging task of forecasting future frames based solely on given past frames in an unsupervised manner [36]. By ingesting raw sequential data, these self-supervised models can uncover intricate spatial and temporal interdependencies without the need for tedious manual annotation, enabling them to extrapolate coherently into the future in a realistic fashion [26, 11]. Spatio-temporal predictive learning benefits a wide range of applications with its ability to anticipate the future from the past in a data-driven way, including modeling the devastating impacts of climate change [34, 32], predicting human movement [53, 41], forecasting traffic flow in transportation systems [7, 47], and learning expressive representations from video [29, 17]. By learning to predict the future without supervision from massive datasets, these techniques have the potential to transform domains where anticipation and planning are crucial but limited labeled data exists [8, 2, 40, 28].

Despite the significance of spatio-temporal predictive learning and the development of various approaches, there remains a conspicuous lack of a comprehensive benchmark for this field. We

\*Equal contribution.

†Corresponding author.

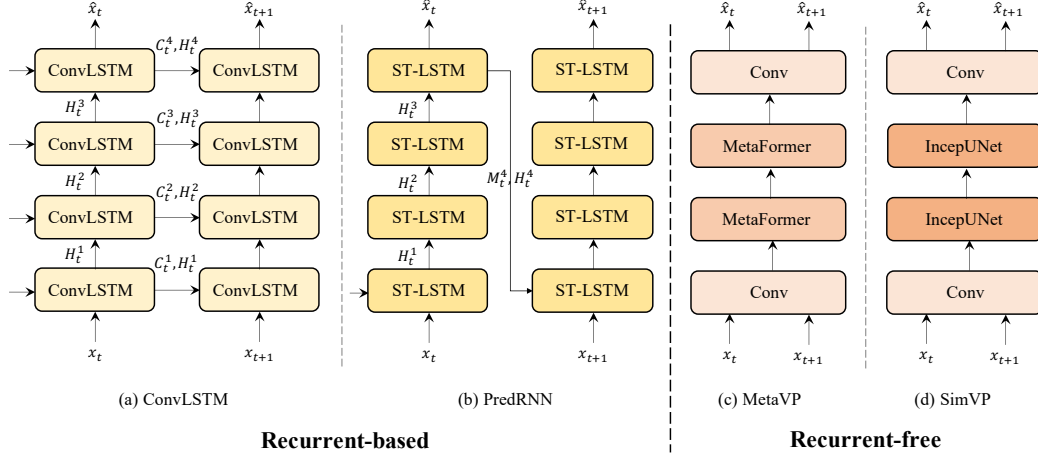


Figure 1: Two typical spatio-temporal predictive learning models.

believe that a comprehensive benchmark is essential for advancing the field and facilitating meaningful comparisons between different methods. In particular, there exists a perennial question that has not yet been conclusively answered: *is it necessary to employ recurrent neural network architectures to capture temporal dependencies?* In other words, *can recurrent-free models achieve performance comparable to recurrent-based models without explicit temporal modeling?*

Since the seminal work ConvLSTM [34] was proposed, which ingeniously integrates convolutional networks and long-short term memory (LSTM) networks [13] to separately capture spatial and temporal correlations, researchers have vacillated between utilizing or eschewing recurrent architectures. As shown in Figure 1, (a) ConvLSTM is a prototypical recurrent-based model that infuses a recurrent structure into convolutional networks. (b) PredRNN [45] represents a series of recurrent models that revise the flow of information to enhance performance. (c) MetaVP is the recurrent-free model that abstracted from SimVP by substituting its IncepU [9] modules with MetaFormers [51]. (d) SimVP [9, 36] is a typical recurrent-free model that achieves performance comparable to previous state-of-the-art models without explicitly modeling temporal dependencies.

In this study, we illuminate the long-standing question of whether explicit temporal modeling with recurrent neural networks is requisite for spatio-temporal predictive learning. To achieve this, we present a comprehensive benchmark called OpenSTL (**O**pen **S**patio-**T**emporal predictive Learning). We revisit the approaches that represent the foremost strands within a modular and extensive framework to ensure fair comparisons. We summarize our main contributions as follows:

- We build OpenSTL, a comprehensive benchmark for spatio-temporal predictive learning that includes 14 representative algorithms and 24 models. OpenSTL covers a wide range of methods and classifies them into two categories: recurrent-based and recurrent-free methods.
- We conduct extensive experiments on a diversity of tasks ranging from synthetic moving object trajectories to real-world human motion, driving scenes, traffic flow, and weather forecasting. The datasets span synthetic to real-world data and micro-to-macro scales.
- While recurrent-based models have been well developed, we rethink the potential of recurrent-free models based on insights from OpenSTL. We propose generalizing MetaFormer-like architectures [51] to boost recurrent-free spatio-temporal predictive learning. Recurrent-free models can thus reformulate the problem as a downstream task of designing vision backbones for general applications.

## 2 Background and Related work

### 2.1 Problem definition

We propose the formal definition for the spatio-temporal predictive learning problem as follows. Given a sequence of video frames  $\mathcal{X}^{t,T} = \{\mathbf{x}^i\}_{t-T+1}^t$  up to time  $t$  spanning the past  $T$  frames, the objective is to predict the subsequent  $T'$  frames  $\mathcal{Y}^{t+1,T'} = \{\mathbf{x}^i\}_{t+1}^{t+1+T'}$  from time  $t+1$  onwards, where each frame  $\mathbf{x}_i \in \mathbb{R}^{C \times H \times W}$  typically comprises  $C$  channels, with height  $H$  and width  $W$  pixels. In practice, we represent the input sequence of observed frames and output sequence of predicted frames respectively as tensors  $\mathcal{X}^{t,T} \in \mathbb{R}^{T \times C \times H \times W}$  and  $\mathcal{Y}^{t+1,T'} \in \mathbb{R}^{T' \times C \times H \times W}$ .

The model with learnable parameters  $\Theta$  learns a mapping  $\mathcal{F}_\Theta : \mathcal{X}^{t,T} \mapsto \mathcal{Y}^{t+1,T'}$  by leveraging both spatial and temporal dependencies. In our case, the mapping  $\mathcal{F}_\Theta$  corresponds to a neural network trained to minimize the discrepancy between the predicted future frames and the ground-truth future frames. The optimal parameters  $\Theta^*$  are given by:

$$\Theta^* = \arg \min_{\Theta} \mathcal{L}(\mathcal{F}_\Theta(\mathcal{X}^{t,T}), \mathcal{Y}^{t+1,T'}), \quad (1)$$

where  $\mathcal{L}$  denotes a loss function that quantifies such discrepancy.

In this study, we categorize prevalent spatio-temporal predictive learning methods into two classes: recurrent-based and recurrent-free models. For *recurrent-based models*, the mapping  $\mathcal{F}_\Theta$  comprises several recurrent interactions:

$$\mathcal{F}_\Theta : f_\theta(\mathbf{x}^{t-T+1}, \mathbf{h}^{t-T+1}) \circ \dots \circ f_\theta(\mathbf{x}^t, \mathbf{h}^t) \circ \dots \circ f_\theta(\mathbf{x}^{t+T'-1}, \mathbf{h}^{t+T'-1}), \quad (2)$$

where  $\mathbf{h}^i$  represents the memory state encompassing historical information and  $f_\theta$  denotes the mapping between each pair of adjacent frames. The parameters  $\theta$  are shared across each state. Therefore, the prediction process can be expressed as follows:

$$\mathbf{x}^{t+1} = f_\theta(\mathbf{x}^i, \mathbf{h}^i), \forall i \in \{t+1, \dots, t+T'\}, \quad (3)$$

For *recurrent-free models*, the prediction process directly feeds the whole sequence of observed frames into the model and outputs the complete predicted frames at once.

### 2.2 Recurrent-based models

Since the pioneering work ConvLSTM [34] was proposed, recurrent-based models [26, 27, 14, 11, 50, 28] have been extensively studied. PredRNN [45] adopts vanilla ConvLSTM modules to build a Spatio-temporal LSTM (ST-LSTM) unit that models spatial and temporal variations simultaneously. PredRNN++ [43] proposes a gradient highway unit to mitigate the gradient vanishing and a Casual-LSTM module to cascadelly connect spatial and temporal memories. PredRNNv2 [46] further proposes a curriculum learning strategy and a memory decoupling loss to boost performance. MIM [47] introduces high-order non-stationarity learning in designing LSTM modules. PhyDNet [11] explicitly disentangles PDE dynamics from unknown complementary information with a recurrent physical unit. E3DLSTM [44] integrates 3D convolutions into recurrent networks. MAU [3] proposes a motion-aware unit that captures motion information. Although various recurrent-based models have been developed, the reasons behind their strong performance remain not fully understood.

### 2.3 Recurrent-free models

Compared to recurrent-based models, recurrent-free models have received less attention. Previous studies tend to use 3D convolutional networks to model temporal dependencies [25, 1]. PredCNN [49] and TrajectoryCNN [22] use 2D convolutional networks for efficiency. However, early recurrent-free models were doubted due to their relatively poor performance. Recently, SimVP [9, 36, 37] provided a simple but effective recurrent-free baseline with competitive performance. In this study, we implemented representative recurrent-based and recurrent-free models under a unified framework to systematically investigate their intrinsic properties. Moreover, we further explored the potential of recurrent-free models by reformulating the spatio-temporal predictive learning problem and extending MetaFormers [51] to bridge the gap between the visual backbone and spatio-temporal learning.

### 3 OpenSTL

#### 3.1 Supported Methods

##### 3.1.1 Overview

OpenSTL has implemented 14 representative spatio-temporal predictive learning methods under a unified framework, including 11 recurrent-based methods and 3 recurrent-free methods. We summarize these methods in Table 1, where we also provide the corresponding conference/journal and the types of their spatial-temporal modeling components. The spatial modeling of these methods is fundamentally consistent. Most methods apply two-dimensional convolutional networks (Conv2D) to model spatial dependencies, while E3D-LSTM and CrevNet harness three-dimensional convolutional networks (Conv3D) instead.

The primary distinction between these methods lies in how they model temporal dependencies using their proposed modules. The ST-LSTM module, proposed in PredRNN [45], is the most widely used module. CrevNet has a similar modeling approach as PredRNN, but it incorporates an information-preserving mechanism into the model. Analogously, Casual-LSTM [43], MIM Block [47], E3D-LSTM [44], PhyCell [11], and MAU [3] represent variants of ConvLSTM proposed with miscellaneous motivations. MVFB is built as a multi-scale voxel flow block that diverges from ConvLSTM. However, DMVFN [15] predicts future frames frame-by-frame which still qualifies as a recurrent-based model. IncepU [9] constitutes an Unet-like module that also exploits the multi-scale feature from the InceptionNet-like architecture. gSTA [36] and TAU [37] extend the IncepU module to simpler and more efficient architectures without InceptionNet or Unet-like architectures. In this work, we further extend the temporal modeling of recurrent-free models by introducing MetaFormers [51] to boost recurrent-free spatio-temporal predictive learning.

Table 1: Categorizations of the supported spatial-temporal predictive learning methods in OpenSTL.

Category	Method	Conference/Journal	Spatial modeling	Temporal modeling
Recurrent-based	ConvLSTM [34]	NeurIPS 2015	Conv2D	Conv-LSTM
	PredNet [26]	ICLR 2017	Conv2D	ST-LSTM
	PredRNN [45]	NeurIPS 2017	Conv2D	ST-LSTM
	PredRNN++ [43]	ICML 2018	Conv2D	Casual-LSTM
	MIM [47]	CVPR 2019	Conv2D	MIM Block
	E3D-LSTM [44]	ICLR 2019	Conv3D	E3D-LSTM
	CrevNet [50]	ICLR 2020	Conv3D	ST-LSTM
	PhyDNet [11]	CVPR 2020	Conv2D	ConvLSTM+PhyCell
	MAU [3]	NeurIPS 2021	Conv2D	MAU
	PredRNNv2 [46]	TPAMI 2022	Conv2D	ST-LSTM
Recurrent-free	DMVFN [15]	CVPR 2023	Conv2D	MVFB
	SimVP [9]	CVPR 2022	Conv2D	IncepU
	TAU [37]	CVPR 2023	Conv2D	TAU
	SimVPv2 [36]	arXiv	Conv2D	gSTA

##### 3.1.2 Rethink the recurrent-free models

Although less studied, recurrent-free spatio-temporal predictive learning models share a similar architecture, as illustrated in Figure 2. The encoder comprises several 2D convolutional networks, which project high-dimensional input data into a low-dimensional latent space. When given a batch of input observed frames  $\mathcal{B} \in \mathbb{R}^{B \times T \times C \times H \times W}$ , the encoder focuses solely on intra-frame spatial correlations, ignoring temporal modeling. Subsequently, the middle temporal module stacks the low-dimensional representations along the temporal dimension to ascertain temporal dependencies. Finally, the decoder comprises several 2D convolutional upsampling networks, which reconstruct subsequent frames from the learned latent representations.

The encoder and decoder enable efficient temporal learning by modeling temporal dependencies in a low-dimensional latent space. The core component of recurrent-free models is the temporal module. Previous studies have proposed temporal modules such as IncepU [9], TAU [37], and



gSTA [36] that have proved beneficial. However, we argue that the competence stems primarily from the general recurrent-free architecture instead of the specific temporal modules. Thus, we employ MetaFormers [51] as the temporal module by changing the input channels from the original  $C$  to inter-frame channels  $T \times C$ . By extending the recurrent-free architecture, we leverage the advantages of MetaFormers to enhance the recurrent-free model. In this work, we implement ViT [6], Swin Transformer [23], Uniformer [19], MLP-Mixer [38], ConvMixer [39], Poolformer [51], ConvNeXt [24], VAN [12], HorNet [30], and MogaNet [20] for the MetaFormers-based recurrent-free model, substituting the intermediate temporal module in the original recurrent-free architecture.

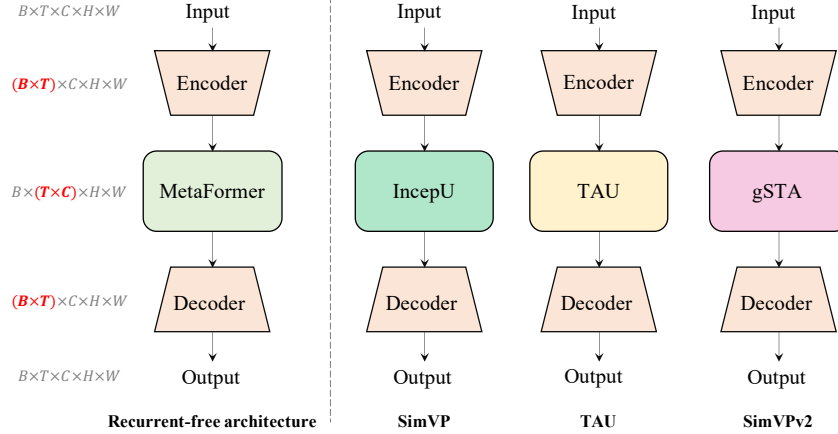


Figure 2: The general architecture of recurrent-free models.

### 3.2 Supported Tasks

We have curated five diverse tasks in our OpenSTL benchmark, which cover a wide range of scenarios from synthetic simulations to real-world situations at various scales. The tasks include: synthetic moving object trajectories, real-world human motion capture, driving scenes, traffic flow, and weather forecasting. The datasets used in our benchmark range from synthetic to real-world, and from micro to macro scales. We have provided a summary of the dataset statistics in Table 2.

Table 2: The detailed dataset statistics of the supported tasks in OpenSTL.

Dataset	Training size	Testing size	Channel	Height	Width	$T$	$T'$
Moving MNIST	10,000	10,000	1	64	64	10	10
KTH	4,940	3,030	1	128	128	10	20/40
Human3.6M	73,404	8,582	3	128	128	4	4
Kitti&Caltech	3,160	3,095	3	128	160	10	1
TaxiBJ	20,461	500	2	32	32	4	4
WeatherBench-S	2,167	706	1	32/128	64/256	12	12
WeatherBench-M	54,019	2,883	4	32	64	4	4

**Synthetic moving object trajectory prediction** *Moving MNIST* [35] is one of the seminal benchmark datasets that has been extensively utilized. Each video sequence comprises two moving digits confined within a  $64 \times 64$  frame. Each digit was assigned a velocity whose direction was randomly chosen from a unit circle and whose magnitude was also arbitrarily selected from a fixed range. Apart from the original Moving MNIST dataset, we provide two variants with more complicated objects (*Moving FashionMNIST*) that replace the digits with fashion objects and more complex scenes (*Moving MNIST-CIFAR*) that employ images from the CIFAR-10 dataset [18] as the background.

**Human motion capture** Predicting human motion is challenging due to the complexity of human movements, which vary greatly among individuals and actions. We utilized the *KTH* dataset [33], which includes six types of human actions: walking, jogging, running, boxing, hand waving, and hand clapping. We furnish two settings, predicting the next 20 and 40 frames respectively. *Human3.6M* [16] is an intricate human pose dataset containing high-resolution RGB videos. Analogous to preceding studies [11, 47], we predict the next four frames by the observed four frames.

**Driving scene prediction** Predicting the future dynamics of driving scenarios is crucial for autonomous driving. Compared to other tasks, this undertaking involves non-stationary and diverse scenes. To address this issue, we follow the conventional approach [26] and train the model on the *Kitti* [10] dataset. We then evaluate the performance on the *Caltech Pedestrian* [5] dataset. To ensure consistency, we center-cropped and downsized all frames to  $128 \times 160$  pixels.

**Traffic flow prediction** Forecasting the dynamics of crowds is crucial for traffic management and public safety. To evaluate spatio-temporal predictive learning approaches for traffic flow prediction, we use the *TaxiBJ* [52] dataset. This dataset includes GPS data from taxis and meteorological data in Beijing. The dataset contains two types of crowd flows, representing inflow and outflow. The temporal interval is 30 minutes, and the spatial resolution is  $32 \times 32$ .

**Weather forecasting** Global weather pattern prediction is an essential natural predicament. The WeatherBench [31] dataset is a large-scale weather forecasting dataset encompassing various types of climatic factors. The raw data is re-grid to  $5.625^\circ$  resolution ( $32 \times 64$  grid points) and  $1.40625^\circ$  ( $128 \times 256$  grid points). We consider two setups: First, *WeatherBench-S* is a single-variable setup in which each climatic factor is trained independently. The model is trained on data from 2010-2015, validated on data from 2016, and tested on data from 2017-2018, with a one-hour temporal interval. Second, *WeatherBench-M* is a multi-variable setup that mimics real-world weather forecasting more closely. All climatic factors are trained simultaneously. The model is trained on data from 1979 to 2015, using the same validation and testing data as WeatherBench-S. The temporal interval is extended to six hours, capturing a broader range of temporal dependencies.

### 3.3 Evaluation Metrics

We evaluate the performance of supported models on the aforementioned tasks using various metrics in a thorough and rigorous manner. We use them for specific tasks according to their characteristics.

**Error metrics** We utilize the mean squared error (MSE) and mean absolute error (MAE) to evaluate the difference between the predicted results and the true targets. Root mean squared error (RMSE) is also used in weather forecasting as it is more common in this domain.

**Similarity metrics** We utilize the structural similarity index measure (SSIM) [48] and peak signal-to-noise ratio (PSNR) to evaluate the similarity between the predicted results and the true targets. Such metrics are extensively used in image processing and computer vision.

**Perceptual metrics** LPIPS [54] is implemented to evaluate the perceptual difference between the predicted results and the true targets in the human visual system. LPIPS provides a perceptually-aligned evaluation for vision tasks. We utilize this metric in real-world video prediction tasks.

**Computational metrics** We utilize the number of parameters and the number of floating-point operations (FLOPs) to evaluate the computational complexity of the models. We also report the frames per second (FPS) on a single NVIDIA V100 GPU to evaluate the inference speed.

### 3.4 Codebase Structure

While existing open-sourced spatio-temporal predictive learning codebases are independent, OpenSTL provides a modular and extensible framework that adheres to the design principles of OpenMMLab [4] and assimilates code elements from OpenMixup [21] and USB [42]. OpenSTL excels in user-friendliness, organization, and comprehensiveness, surpassing the usability of existing open-source STL codebases. A detailed description of the codebase structure can be found in Appendix B.

## 4 Experiment and Analysis

We conducted comprehensive experiments on the mentioned tasks to assess the performance of the supported methods in OpenSTL. Detailed analysis of the results is presented to gain insights into spatio-temporal predictive learning. Implementation details can be found in Appendix C.

#### 4.1 Synthetic Moving Object Trajectory Prediction

We conduct experiments on the synthetic moving object trajectory prediction task, utilizing three datasets: Moving MNIST, Moving FashionMNIST, and Moving MNIST-CIFAR. The performance of the evaluated models on the Moving MNIST dataset is reported in Table 3. The detailed results for the other two synthetic datasets are in Appendix D.1.

It can be observed that recurrent-based models yield varied results that do not consistently outperform recurrent-free models, while recurrent-based models always exhibit slower inference speeds than their recurrent-free counterparts. Although PredRNN, PredRNN++, MIM, and PredRNNv2 achieve lower MSE and MAE values compared to recurrent-free models, their FLOPs are nearly five times higher, and their FPS are approximately seven times slower than all recurrent-free models. Furthermore, there are minimal disparities in the performance of recurrent-free models as opposed to recurrent-based models, highlighting the robustness of the proposed general recurrent-free architecture. The remaining two synthetic datasets, consisting of more intricate moving objects (Moving FashionMNIST) and complex scenes (Moving MNIST-CIFAR), reinforce the experimental findings that recurrent-free models deliver comparable performance with significantly higher efficiency. In these toy datasets characterized by high frequency but low resolution, recurrent-based models excel in capturing temporal dependencies but are susceptible to high computational complexity.

Table 3: The performance on the Moving MNIST dataset.

	Method	Params (M)	FLOPs (G)	FPS	MSE ↓	MAE ↓	SSIM ↑	PSNR ↑
Recurrent-based	ConvLSTM	15.0	56.8	113	29.80	90.64	0.9288	22.10
	PredNet	12.5	8.4	659	161.38	201.16	0.7783	14.67
	PredRNN	23.8	116.0	54	23.97	72.82	0.9462	23.28
	PredRNN++	38.6	171.7	38	<b>22.06</b>	<b>69.58</b>	<b>0.9509</b>	<b>23.65</b>
	MIM	38.0	179.2	37	22.55	69.97	0.9498	23.56
	E3D-LSTM	51.0	298.9	18	35.97	78.28	0.9320	21.11
	CrevNet	5.0	270.7	10	30.15	86.28	0.9350	22.15
	PhyDNet	3.1	15.3	182	28.19	78.64	0.9374	22.62
	MAU	4.5	17.8	201	26.86	78.22	0.9398	22.57
	PredRNNv2	23.9	116.6	52	24.13	73.73	0.9453	23.21
Recurrent-free	DMVFN	3.5	0.2	1145	123.67	179.96	0.8140	16.15
	SimVP	58.0	19.4	209	32.15	89.05	0.9268	21.84
	TAU	44.7	16.0	283	24.60	71.93	0.9454	23.19
	SimVPv2	46.8	16.5	282	26.69	77.19	0.9402	22.78
	ViT	46.1	16.9	290	35.15	95.87	0.9139	21.67
	Swin Transformer	46.1	16.4	294	29.70	84.05	0.9331	22.22
	Uniformer	44.8	16.5	296	30.38	85.87	0.9308	22.13
	MLP-Mixer	38.2	14.7	334	29.52	83.36	0.9338	22.22
	ConvMixer	3.9	5.5	658	32.09	88.93	0.9259	21.93
	Poolformer	37.1	14.1	341	31.79	88.48	0.9271	22.03
	ConvNext	37.3	14.1	344	26.94	77.23	0.9397	22.74
	VAN	44.5	16.0	288	26.10	76.11	0.9417	22.89
	HorNet	45.7	16.3	287	29.64	83.26	0.9331	22.26
	MogaNet	46.8	16.5	255	25.57	75.19	0.9429	22.99

#### 4.2 Real-world Video Prediction

We perform experiments on real-world video predictions, specifically focusing on human motion capturing using the KTH and Human3.6M datasets, as well as driving scene prediction using the Kitti&Caltech dataset. Due to space constraints, we present the results for the Kitti&Caltech dataset in Table 4, while the detailed results for the other datasets can be found in Appendix D.2. We observed that as the resolution increases, the computational complexity of recurrent-based models dramatically increases. In contrast, recurrent-free models achieve a commendable balance between efficiency and performance. Notably, although some recurrent-based models achieve lower MSE and MAE values,

their FLOPs are nearly 20 times higher compared to their recurrent-free counterparts. This highlights the efficiency advantage of recurrent-free models, especially in high-resolution scenarios.

Table 4: The performance on the Kitti&Caltech dataset.

	Method	Params (M)	FLOPs (G)	FPS	MSE ↓	MAE ↓	SSIM ↑	PSNR ↑	LPIPS ↓
Recurrent-based	ConvLSTM	15.0	595.0	33	139.6	1583.3	0.9345	27.46	8.58
	PredNet	12.5	42.8	94	159.8	1568.9	0.9286	27.21	11.29
	PredRNN	23.7	1216.0	17	130.4	1525.5	0.9374	27.81	7.40
	PredRNN++	38.5	1803.0	12	<b>125.5</b>	<b>1453.2</b>	0.9433	28.02	13.21
	MIM	49.2	1858.0	39	125.1	1464.0	0.9409	<b>28.10</b>	6.35
	E3D-LSTM	54.9	1004.0	10	200.6	1946.2	0.9047	25.45	12.60
	PhyDNet	3.10	40.4	117	312.2	2754.8	0.8615	23.26	32.19
	MAU	24.3	172.0	16	177.8	1800.4	0.9176	26.14	9.67
	PredRNNv2	23.8	1223.0	16	147.8	1610.5	0.9330	27.12	8.92
	DMVFN	3.6	1.2	557	183.9	1531.1	0.9314	26.78	<b>4.94</b>
Recurrent-free	SimVP	8.6	60.6	57	160.2	1690.8	0.9338	26.81	6.76
	TAU	15.0	92.5	55	131.1	1507.8	0.9456	27.83	5.49
	SimVPv2	15.6	96.3	40	129.7	1507.7	0.9454	27.89	5.57
	ViT	12.7	155.0	25	146.4	1615.8	0.9379	27.43	6.66
	Swin Transformer	15.3	95.2	49	155.2	1588.9	0.9299	27.25	8.11
	Unifomer	11.8	104.0	28	135.9	1534.2	0.9393	27.66	6.87
	MLP-Mixer	22.2	83.5	60	207.9	1835.9	0.9133	26.29	7.75
	ConvMixer	1.5	23.1	129	174.7	1854.3	0.9232	26.23	7.76
	Poolformer	12.4	79.8	51	153.4	1613.5	0.9334	27.38	7.00
	ConvNext	12.5	80.2	54	146.8	1630.0	0.9336	27.19	6.99
	VAN	14.9	92.5	41	127.5	1476.5	0.9462	27.98	5.50
	HorNet	15.3	94.4	43	152.8	1637.9	0.9365	27.09	6.00
	MogaNet	15.6	96.2	36	131.4	1512.1	<b>0.9442</b>	27.79	5.39

### 4.3 Traffic and Weather Forecasting

Traffic flow prediction and weather forecasting are two critical tasks that have significant implications for public safety and scientific research. While these tasks operate at a macro level, they exhibit lower frequencies compared to the tasks mentioned above, and the states along the timeline tend to be more stable. Capturing subtle changes in such tasks poses a significant challenge. In order to assess the performance of the supported models in OpenSTL, we conduct experiments on the TaxiBJ and WeatherBench datasets. It is worth noting that weather forecasting encompasses various settings, and we provide detailed results of them in Appendix D.3.

Here, we present a comparison of the MAE and RMSE metrics for representative approaches in single-variable weather factor forecasting at low resolution. Figure 3 displays the results for four climatic factors, i.e., temperature, humidity, wind component, and cloud cover. Notably, recurrent-free models consistently outperform recurrent-based models across all weather factors, indicating their potential to apply spatio-temporal predictive learning to macro-scale tasks instead of relying solely on recurrent-based models. These findings underscore the promising nature of recurrent-free models and suggest that they can be a viable alternative to the prevailing recurrent-based models in the context of weather forecasting. Furthermore, in the Appendix, we provide additional insights into high-resolution and multi-variable weather forecasting, where similar trends are observed.

## 5 Conclusion and Discussion

This paper introduces OpenSTL, a comprehensive benchmark for spatio-temporal predictive learning with a diverse set of 14 representative methods and 24 models, addressing a wide range of challenging tasks. OpenSTL categorizes existing approaches into recurrent-based and recurrent-free models. To unlock the potential of recurrent-free models, we propose a general recurrent-free architecture and introduce MetaFormers for temporal modeling. Extensive experiments are conducted to systematically evaluate the performance of the supported models across various tasks. In synthetic datasets, recurrent-based models excel at capturing temporal dependencies, while recurrent-free

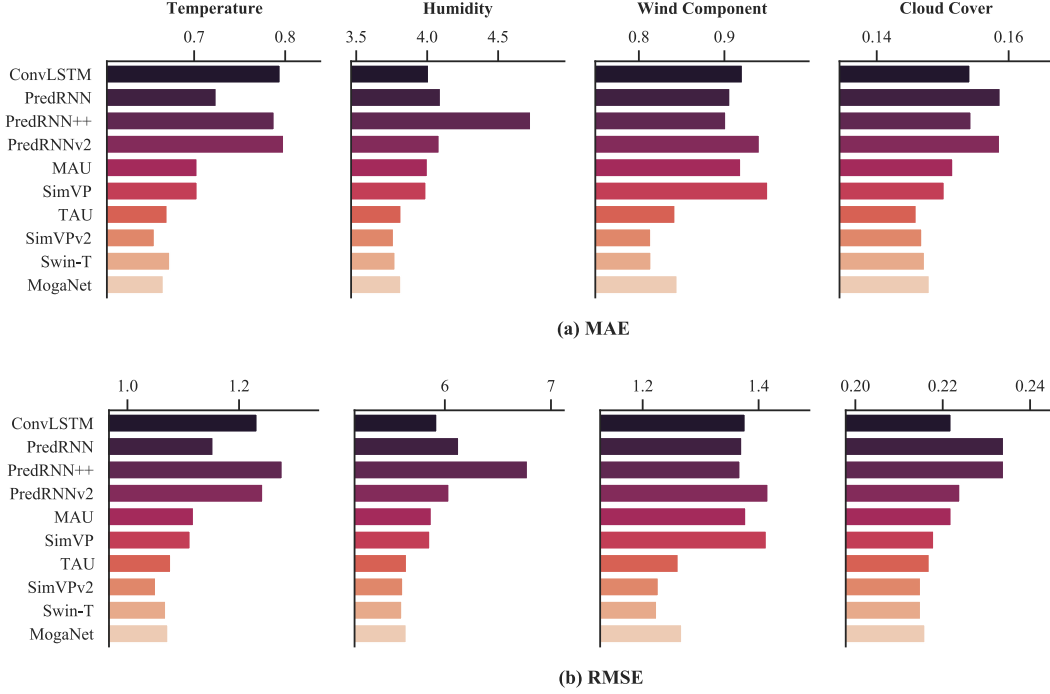


Figure 3: The (a) MAE and (b) RMSE metrics of the representative approaches on the four weather forecasting tasks in WeatherBench.

models achieve comparable performance with significantly higher efficiency. In real-world video prediction tasks, recurrent-free models strike a commendable balance between efficiency and performance. Additionally, recurrent-free models demonstrate significant superiority over their counterparts in weather forecasting, highlighting their potential for scientific applications at a macro-scale level.

Moreover, we observed that *recurrent architectures are beneficial in capturing temporal dependencies, but they are not always necessary, especially for computationally expensive tasks*. Recurrent-free models can be a viable alternative that provides a good balance between efficiency and performance. The effectiveness of recurrent-based models in capturing high-frequency spatio-temporal dependencies can be attributed to their sequential tracking of frame-by-frame changes, providing a local temporal inductive bias. On the other hand, recurrent-free models combine multiple frames together, exhibiting a global temporal inductive bias that is suitable for low-frequency spatio-temporal dependencies. We hope that our work provides valuable insights and serves as a reference for future research.

While our primary focus lies in general spatio-temporal predictive learning, there are still several open problems that require further investigation. One particular challenge is finding ways to effectively leverage the strengths of both recurrent-based and recurrent-free models to enhance the modeling of spatial-temporal dependencies. While there is a correspondence between the spatial encoding and temporal modeling in MetaVP and the token mixing and channel mixing in MetaFormer, it raises the question of whether we can improve recurrent-free models by extending the existing MetaFormers.

## Acknowledgments and Disclosure of Funding

This work was supported by the National Key R&D Program of China (2022ZD0115100), the National Natural Science Foundation of China (U21A20427), the Competitive Research Fund (WU2022A009) from the Westlake Center for Synthetic Biology and Integrated Bioengineering.

## References

- [1] S. Aigner and M. Körner. Futuregan: Anticipating the future frames of video sequences using spatio-temporal 3d convolutions in progressively growing gans. *arXiv preprint*

- arXiv:1810.01325*, 2018.
- [2] L. Castrejon, N. Ballas, and A. Courville. Improved conditional vrnnns for video prediction. In *Proceedings of the IEEE/CVF International Conference on Computer Vision*, pages 7608–7617, 2019.
  - [3] Z. Chang, X. Zhang, S. Wang, S. Ma, Y. Ye, X. Xinguang, and W. Gao. Mau: A motion-aware unit for video prediction and beyond. *Advances in Neural Information Processing Systems*, 34, 2021.
  - [4] M. Contributors. MMCV: OpenMMLab computer vision foundation. <https://github.com/open-mmlab/mmcv>, 2018.
  - [5] P. Dollár, C. Wojek, B. Schiele, and P. Perona. Pedestrian detection: A benchmark. In *CVPR*, June 2009.
  - [6] A. Dosovitskiy, L. Beyer, A. Kolesnikov, D. Weissenborn, X. Zhai, T. Unterthiner, M. Dehghani, M. Minderer, G. Heigold, S. Gelly, et al. An image is worth 16x16 words: Transformers for image recognition at scale. In *International Conference on Learning Representations*.
  - [7] S. Fang, Q. Zhang, G. Meng, S. Xiang, and C. Pan. Gstnet: Global spatial-temporal network for traffic flow prediction. In *IJCAI*, pages 2286–2293, 2019.
  - [8] C. Finn, I. Goodfellow, and S. Levine. Unsupervised learning for physical interaction through video prediction. *Advances in Neural Information Processing Systems*, 29, 2016.
  - [9] Z. Gao, C. Tan, and S. Z. Li. Simvp: Simpler yet better video prediction. In *Proceedings of the IEEE/CVF Conference on Computer Vision and Pattern Recognition*, pages 3170–3180, 2022.
  - [10] A. Geiger, P. Lenz, C. Stiller, and R. Urtasun. Vision meets robotics: The kitti dataset. *The International Journal of Robotics Research*, 32(11):1231–1237, 2013.
  - [11] V. L. Guen and N. Thome. Disentangling physical dynamics from unknown factors for unsupervised video prediction. In *Proceedings of the IEEE/CVF Conference on Computer Vision and Pattern Recognition*, pages 11474–11484, 2020.
  - [12] M.-H. Guo, C.-Z. Lu, Z.-N. Liu, M.-M. Cheng, and S.-M. Hu. Visual attention network. *arXiv preprint arXiv:2202.09741*, 2022.
  - [13] S. Hochreiter and J. Schmidhuber. Long short-term memory. *Neural computation*, 9(8):1735–1780, 1997.
  - [14] J.-T. Hsieh, B. Liu, D.-A. Huang, L. F. Fei-Fei, and J. C. Niebles. Learning to decompose and disentangle representations for video prediction. *Advances in Neural Information Processing Systems*, 31, 2018.
  - [15] X. Hu, Z. Huang, A. Huang, J. Xu, and S. Zhou. A dynamic multi-scale voxel flow network for video prediction. In *Proceedings of the IEEE/CVF Conference on Computer Vision and Pattern Recognition (CVPR)*, 2023.
  - [16] C. Ionescu, D. Papava, V. Olaru, and C. Sminchisescu. Human3.6m: Large scale datasets and predictive methods for 3d human sensing in natural environments. *IEEE transactions on pattern analysis and machine intelligence*, 36(7):1325–1339, 2013.
  - [17] S. Jenni, G. Meishvili, and P. Favaro. Video representation learning by recognizing temporal transformations. In *European Conference on Computer Vision*, pages 425–442. Springer, 2020.
  - [18] A. Krizhevsky, G. Hinton, et al. Learning multiple layers of features from tiny images. 2009.
  - [19] K. Li, Y. Wang, J. Zhang, P. Gao, G. Song, Y. Liu, H. Li, and Y. Qiao. Uniformer: Unifying convolution and self-attention for visual recognition. *arXiv preprint arXiv:2201.09450*, 2022.
  - [20] S. Li, Z. Wang, Z. Liu, C. Tan, H. Lin, D. Wu, Z. Chen, J. Zheng, and S. Z. Li. Efficient multi-order gated aggregation network. *arXiv preprint arXiv:2211.03295*, 2022.
  - [21] S. Li, Z. Wang, Z. Liu, D. Wu, C. Tan, and S. Z. Li. Openmixup: Open mixup toolbox and benchmark for visual representation learning. *ArXiv*, abs/2209.04851, 2022.
  - [22] X. Liu, J. Yin, J. Liu, P. Ding, J. Liu, and H. Liu. Trajectorycnn: a new spatio-temporal feature learning network for human motion prediction. *IEEE Transactions on Circuits and Systems for Video Technology*, 31(6):2133–2146, 2020.



- [23] Z. Liu, Y. Lin, Y. Cao, H. Hu, Y. Wei, Z. Zhang, S. Lin, and B. Guo. Swin transformer: Hierarchical vision transformer using shifted windows. In *Proceedings of the IEEE/CVF International Conference on Computer Vision*, pages 10012–10022, 2021.
- [24] Z. Liu, H. Mao, C.-Y. Wu, C. Feichtenhofer, T. Darrell, and S. Xie. A convnet for the 2020s. *arXiv preprint arXiv:2201.03545*, 2022.
- [25] Z. Liu, R. A. Yeh, X. Tang, Y. Liu, and A. Agarwala. Video frame synthesis using deep voxel flow. In *Proceedings of the IEEE International Conference on Computer Vision*, pages 4463–4471, 2017.
- [26] W. Lotter, G. Kreiman, and D. Cox. Deep predictive coding networks for video prediction and unsupervised learning. In *International Conference on Learning Representations*, 2017.
- [27] M. Oliu, J. Selva, and S. Escalera. Folded recurrent neural networks for future video prediction. In *Proceedings of the European Conference on Computer Vision (ECCV)*, pages 716–731, 2018.
- [28] S. Oprea, P. Martinez-Gonzalez, A. Garcia-Garcia, J. A. Castro-Vargas, S. Orts-Escolano, J. Garcia-Rodriguez, and A. Argyros. A review on deep learning techniques for video prediction. *IEEE Transactions on Pattern Analysis and Machine Intelligence*, 2020.
- [29] R. Qian, T. Meng, B. Gong, M.-H. Yang, H. Wang, S. Belongie, and Y. Cui. Spatiotemporal contrastive video representation learning. In *Proceedings of the IEEE/CVF Conference on Computer Vision and Pattern Recognition*, pages 6964–6974, 2021.
- [30] Y. Rao, W. Zhao, Y. Tang, J. Zhou, S. N. Lim, and J. Lu. Hornet: Efficient high-order spatial interactions with recursive gated convolutions. *Advances in Neural Information Processing Systems*, 35:10353–10366, 2022.
- [31] S. Rasp, P. D. Dueben, S. Scher, J. A. Weyn, S. Mouatadid, and N. Thuerey. Weatherbench: a benchmark data set for data-driven weather forecasting. *Journal of Advances in Modeling Earth Systems*, 12(11):e2020MS002203, 2020.
- [32] M. Reichstein, G. Camps-Valls, B. Stevens, M. Jung, J. Denzler, N. Carvalhais, et al. Deep learning and process understanding for data-driven earth system science. *Nature*, 566(7743):195–204, 2019.
- [33] C. Schudt, I. Laptev, and B. Caputo. Recognizing human actions: a local svm approach. In *Proceedings of the 17th International Conference on Pattern Recognition, 2004. ICPR 2004.*, volume 3, pages 32–36. IEEE, 2004.
- [34] X. Shi, Z. Chen, H. Wang, D.-Y. Yeung, W.-K. Wong, and W.-c. Woo. Convolutional lstm network: A machine learning approach for precipitation nowcasting. *Advances in Neural Information Processing Systems*, 28, 2015.
- [35] N. Srivastava, E. Mansimov, and R. Salakhudinov. Unsupervised learning of video representations using lstms. In *International conference on machine learning*, pages 843–852. PMLR, 2015.
- [36] C. Tan, Z. Gao, S. Li, and S. Z. Li. Simvp: Towards simple yet powerful spatiotemporal predictive learning. *arXiv preprint arXiv:2211.12509*, 2022.
- [37] C. Tan, Z. Gao, L. Wu, Y. Xu, J. Xia, S. Li, and S. Z. Li. Temporal attention unit: Towards efficient spatiotemporal predictive learning. In *Proceedings of the IEEE/CVF Conference on Computer Vision and Pattern Recognition*, 2023.
- [38] I. O. Tolstikhin, N. Houlsby, A. Kolesnikov, L. Beyer, X. Zhai, T. Unterthiner, J. Yung, A. Steiner, D. Keysers, J. Uszkoreit, et al. Mlp-mixer: An all-mlp architecture for vision. *Advances in neural information processing systems*, 34:24261–24272, 2021.
- [39] A. Trockman and J. Z. Kolter. Patches are all you need? *arXiv:2201.09792*, 2022.
- [40] R. Villegas, D. Erhan, H. Lee, et al. Hierarchical long-term video prediction without supervision. In *International Conference on Machine Learning*, pages 6038–6046. PMLR, 2018.
- [41] P. Wang, W. Li, P. Ogunbona, J. Wan, and S. Escalera. Rgb-d-based human motion recognition with deep learning: A survey. *Computer Vision and Image Understanding*, 171:118–139, 2018.
- [42] Y. Wang, H. Chen, Y. Fan, W. Sun, R. Tao, W. Hou, R. Wang, L. Yang, Z. Zhou, L.-Z. Guo, et al. Usb: A unified semi-supervised learning benchmark for classification. *Advances in Neural Information Processing Systems*, 35:3938–3961, 2022.

- [43] Y. Wang, Z. Gao, M. Long, J. Wang, and S. Y. Philip. Predrnn++: Towards a resolution of the deep-in-time dilemma in spatiotemporal predictive learning. In *International Conference on Machine Learning*, pages 5123–5132. PMLR, 2018.
- [44] Y. Wang, L. Jiang, M.-H. Yang, L.-J. Li, M. Long, and L. Fei-Fei. Eidetic 3d lstm: A model for video prediction and beyond. In *International conference on learning representations*, 2018.
- [45] Y. Wang, M. Long, J. Wang, Z. Gao, and P. S. Yu. Predrnn: Recurrent neural networks for predictive learning using spatiotemporal lstms. *Advances in Neural Information Processing Systems*, 30, 2017.
- [46] Y. Wang, H. Wu, J. Zhang, Z. Gao, J. Wang, P. S. Yu, and M. Long. Predrnn: A recurrent neural network for spatiotemporal predictive learning. *arXiv preprint arXiv:2103.09504*, 2021.
- [47] Y. Wang, J. Zhang, H. Zhu, M. Long, J. Wang, and P. S. Yu. Memory in memory: A predictive neural network for learning higher-order non-stationarity from spatiotemporal dynamics. In *Proceedings of the IEEE/CVF Conference on Computer Vision and Pattern Recognition*, pages 9154–9162, 2019.
- [48] Z. Wang, A. C. Bovik, H. R. Sheikh, and E. P. Simoncelli. Image quality assessment: from error visibility to structural similarity. *IEEE transactions on image processing*, 13(4):600–612, 2004.
- [49] Z. Xu, Y. Wang, M. Long, J. Wang, and M. KLiss. Predcnn: Predictive learning with cascade convolutions. In *IJCAI*, pages 2940–2947, 2018.
- [50] W. Yu, Y. Lu, S. Easterbrook, and S. Fidler. Efficient and information-preserving future frame prediction and beyond. In *International Conference on Learning Representations*, 2019.
- [51] W. Yu, M. Luo, P. Zhou, C. Si, Y. Zhou, X. Wang, J. Feng, and S. Yan. Metaformer is actually what you need for vision. In *Proceedings of the IEEE/CVF conference on computer vision and pattern recognition*, pages 10819–10829, 2022.
- [52] J. Zhang, Y. Zheng, and D. Qi. Deep spatio-temporal residual networks for citywide crowd flows prediction. In *Thirty-first AAAI conference on artificial intelligence*, 2017.
- [53] L. Zhang, G. Zhu, P. Shen, J. Song, S. Afaq Shah, and M. Bennamoun. Learning spatiotemporal features using 3dcnn and convolutional lstm for gesture recognition. In *Proceedings of the IEEE International Conference on Computer Vision Workshops*, pages 3120–3128, 2017.
- [54] R. Zhang, P. Isola, A. A. Efros, E. Shechtman, and O. Wang. The unreasonable effectiveness of deep features as a perceptual metric. In *Proceedings of the IEEE conference on computer vision and pattern recognition*, pages 586–595, 2018.

## A Installation and Data Preparation

### A.1 Installation

In our GitHub ([github.com/chengtan9907/OpenSTL](https://github.com/chengtan9907/OpenSTL)), we have provided a conda environment setup file for OpenSTL. Users can easily reproduce the environment by executing the following commands:

```
git clone https://github.com/chengtan9907/OpenSTL
cd OpenSTL
conda env create -f environment.yml
conda activate OpenSTL
python setup.py develop \# or "pip install -e ."
```

By following the instructions above, OpenSTL will be installed in development mode, allowing any local code modifications to take effect. Alternatively, users can install it as a PyPi package using `pip install .`, but remember to reinstall it to apply any local modifications.

### A.2 Data Preparation

It is recommended to symlink the dataset root (assuming `$USER_DATA_ROOT`) to `$OpenSTL/data`. If the folder structure of the user is different, the user needs to change the corresponding paths in config files. We provide tools to download and preprocess the datasets in `OpenSTL/tool/prepare_data`.

## B Codebase Overview

In this section, we present a comprehensive overview of the codebase structure of OpenSTL. The codebase is organized into three abstracted layers, namely the core layer, algorithm layer, and user interface layer, arranged from the bottom to the top, as illustrated in Figure 4.

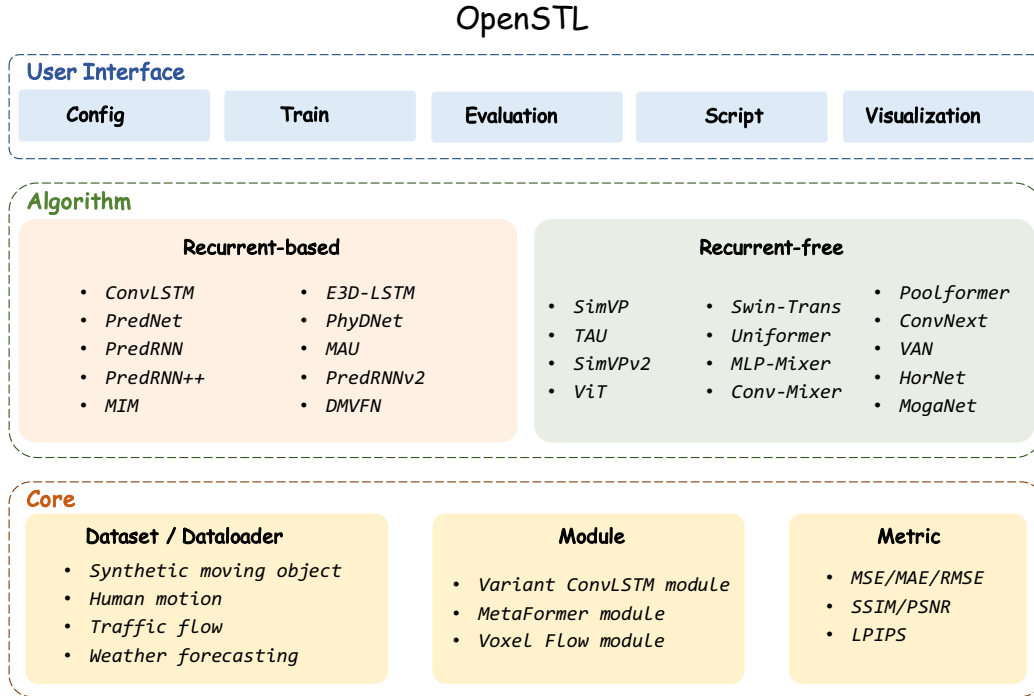


Figure 4: The graphical overview of OpenSTL.

**Core Layer** The core layer comprises essential components of OpenSTL, such as dataloaders for supported datasets, basic modules for supported models, and metrics for evaluation. The dataloaders

offer a unified interface for data loading and preprocessing. The modules consist of foundational unit implementations of supported models. The metrics provide a unified interface for evaluation purposes. The core layer establishes a foundation for the upper layers to ensure flexibility in usage.

**Algorithm Layer** The algorithm layer encompasses the implementations of the supported models, which are organized into two distinct categories: recurrent-based and recurrent-free models. These implementations are developed using the PyTorch framework and closely adhere to the methodologies described in the original research papers and their official open-sourced code. The algorithm layer ensures the compatibility, reliability, and reproducibility of the supported algorithms by abstracting common components and avoiding code duplication, enabling the easy and flexible implementation of customized algorithms. Moreover, the algorithm layer provides a unified interface that facilitates seamless operations such as model training, evaluation, and testing. By offering a consistent interface, the algorithm layer enhances usability and promotes ease of experimentation with the models.

**User Interface Layer** The user interface layer comprises configurations, training, evaluation, and scripts that facilitate the basic usage of OpenSTL. We offer convenient tools for generating visualizations. The user interface layer is designed to be user-friendly and intuitive, enabling users to easily train, evaluate, and test the supported algorithms. By offering detailed parameter settings in the configurations, the user interface layer provides a unified interface that enables users to reproduce the results presented in this paper, without requiring any additional efforts.

## C Implementation Details

Table 5 describes the hyper-parameters employed in the supported models across multiple datasets, namely MMNIST, KITTI, KTH, Human, TaxiBJ, Weather-S, and Weather-M. For each dataset, the hyperparameters include  $T$ ,  $T'$ ,  $\text{hid}_S$ ,  $\text{hid}_T$ ,  $N_S$ ,  $N_T$ , epoch, optimizer, drop path, and learning rate.  $T$  and  $T'$  have the same values for the MMNIST, Human, TaxiBJ, and Weather-M datasets, but differ for KITTI and KTH. The specific values of  $T$  and  $T'$  are depended on the dataset. The learning rate and drop path are chosen from a set of values, and the best result for each experiment is reported.

The parameters  $\text{hid}_S$  and  $\text{hid}_T$  correspond to the size of the hidden layers in the spatial encoder/decoder and the temporal module of the model, respectively. While these parameters exhibit minor variations across datasets, their values largely maintain consistency, underscoring the standardized model structure across diverse datasets.  $N_S$  and  $N_T$  denote the number of blocks in the spatial encoder/decoder and the temporal module, respectively. These four hyper-parameters are from recurrent-free models, we provide the detailed hyper-parameters of recurrent-based models in GitHub for theirs are various. Please refer to the link [OpenSTL/configs](#) for more details.

Table 5: Hyper-parameters of the supported models.

Dataset	MMNIST	KITTI	KTH	Human	TaxiBJ	Weather-S	Weather-M
$T$	10	10	10	4	4	12	4
$T'$	10	1	20	4	4	12	4
$\text{hid}_S$	64	64	64	64	32	32	32
$\text{hid}_T$	512	256	256	512	256	256	256
$N_S$	4	2	2	4	2	2	2
$N_T$	8	6	6	6	8	8	8
epoch	200	100	100	50	50	50	50
optimizer	Adam						
drop path	{0.0, 0.1, 0.2}						
learning rate	{ $1e^{-2}$ , $5e^{-3}$ , $1e^{-3}$ , $5e^{-4}$ , $1e^{-4}$ }						

## D Detailed Experimental Results

### D.1 Synthetic Moving Object Trajectory Prediction

**Moving MNIST** In addition to the quantitative results provided in the main text, we also provide a visualization example for qualitative assessment, as shown in Figure 5. For the convenience of formatting, we arrange the frames vertically from bottom to top. It can be observed that the majority of recurrent-based models produce high-quality predicted results, except for PredNet and DMVFN. Recurrent-free models achieve comparable results but exhibit blurriness in the last few frames. This phenomenon suggests that recurrent-based models excel at capturing temporal dependencies.



Figure 5: The qualitative visualization on Moving MNIST. For the convenience of formatting, we arrange the frames vertically from bottom to top.

**Moving FashionMNIST** We show the quantitative results and qualitative visualization examples in Table 6 and Figure 6, respectively. The results are consistent with those of Moving MNIST, where recurrent-based models perform well in long-range temporal modeling.

Table 6: The performance on the Moving FashionMNIST dataset.

	Method	Params (M)	FLOPs (G)	FPS	MSE ↓	MAE ↓	SSIM ↑	PSNR ↑
Recurrent-based	ConvLSTM	15.0	56.8	113	28.87	113.20	0.8793	22.07
	PredNet	12.5	8.4	659	185.94	318.30	0.6713	14.83
	PredRNN	23.8	116.0	54	22.01	<b>91.74</b>	0.9091	23.42
	PredRNN++	38.6	171.7	38	<b>21.71</b>	91.97	<b>0.9097</b>	<b>23.45</b>
	MIM	38.0	179.2	37	23.09	96.37	0.9043	23.13
	E3D-LSTM	51.0	298.9	18	35.35	110.09	0.8722	21.27
	PhyDNet	3.1	15.3	182	34.75	125.66	0.8567	22.03
	MAU	4.5	17.8	201	26.56	104.39	0.8916	22.51
	PredRNNv2	23.9	116.6	52	24.13	97.46	0.9004	22.96
	DMVFN	3.5	0.2	1145	118.32	220.02	0.7572	16.76
Recurrent-free	SimVP	58.0	19.4	209	30.77	113.94	0.8740	21.81
	TAU	44.7	16.0	283	24.24	96.72	0.8995	22.87
	SimVPv2	46.8	16.5	282	25.86	101.22	0.8933	22.61
	ViT	46.1	16.9	290	31.05	115.59	0.8712	21.83
	Swin Transformer	46.1	16.4	294	28.66	108.93	0.8815	22.08
	Uniformer	44.8	16.5	296	29.56	111.72	0.8779	21.97
	MLP-Mixer	38.2	14.7	334	28.83	109.51	0.8803	22.01
	ConvMixer	3.9	5.5	658	31.21	115.74	0.8709	21.71
	Poolformer	37.1	14.1	341	30.02	113.07	0.8750	21.95
	ConvNext	37.3	14.1	344	26.41	102.56	0.8908	22.49
	VAN	44.5	16.0	288	31.39	116.28	0.8703	22.82
	HorNet	45.7	16.3	287	29.19	110.17	0.8796	22.03
	MogaNet	46.8	16.5	255	25.14	99.69	0.8960	22.73

**Moving MNIST-CIFAR** The quantitative results are presented in Table 7, while the qualitative visualizations are depicted in Figure 7. As the task involves more complex backgrounds, the models are required to pay greater attention to spatial modeling. Consequently, the gap between recurrent-based and recurrent-free models is narrowed.

Table 7: The performance on the Moving MNIST-CIFAR dataset.

	Method	Params (M)	FLOPs (G)	FPS	MSE ↓	MAE ↓	SSIM ↑	PSNR ↑
Recurrent-based	ConvLSTM	15.0	56.8	113	73.31	338.56	0.9204	23.09
	PredNet	12.5	8.4	659	286.70	514.14	0.8139	17.49
	PredRNN	23.8	116.0	54	50.09	225.04	0.9499	24.90
	PredRNN++	38.6	171.7	38	<b>44.19</b>	198.27	<b>0.9567</b>	<b>25.60</b>
	MIM	38.0	179.2	37	48.63	213.44	0.9521	25.08
	E3D-LSTM	51.0	298.9	18	80.79	214.86	0.9314	22.89
	PhyDNet	3.1	15.3	182	142.54	700.37	0.8276	19.92
	MAU	4.5	17.8	201	58.84	255.76	0.9408	24.19
	PredRNNv2	23.9	116.6	52	57.27	252.29	0.9419	24.24
	DMVFN	3.5	0.2	1145	298.73	606.92	0.7765	17.07
Recurrent-free	SimVP	58.0	19.4	209	59.83	214.54	0.9414	24.15
	TAU	44.7	16.0	283	48.17	<b>177.35</b>	0.9539	25.21
	SimVPv2	46.8	16.5	282	51.13	185.13	0.9512	24.93
	ViT	46.1	16.9	290	64.94	234.01	0.9354	23.90
	Swin Transformer	46.1	16.4	294	57.11	207.45	0.9443	24.34
	Uniformer	44.8	16.5	296	56.96	207.51	0.9442	24.38
	MLP-Mixer	38.2	14.7	334	57.03	206.46	0.9446	24.34
	ConvMixer	3.9	5.5	658	59.29	219.76	0.9403	24.17
	Poolformer	37.1	14.1	341	60.98	219.50	0.9399	24.16
	ConvNext	37.3	14.1	344	51.39	187.17	0.9503	24.89
	VAN	44.5	16.0	288	59.59	221.32	0.9398	25.20
	HorNet	45.7	16.3	287	55.79	202.73	0.9456	24.49
	MogaNet	46.8	16.5	255	49.48	184.11	0.9521	25.07



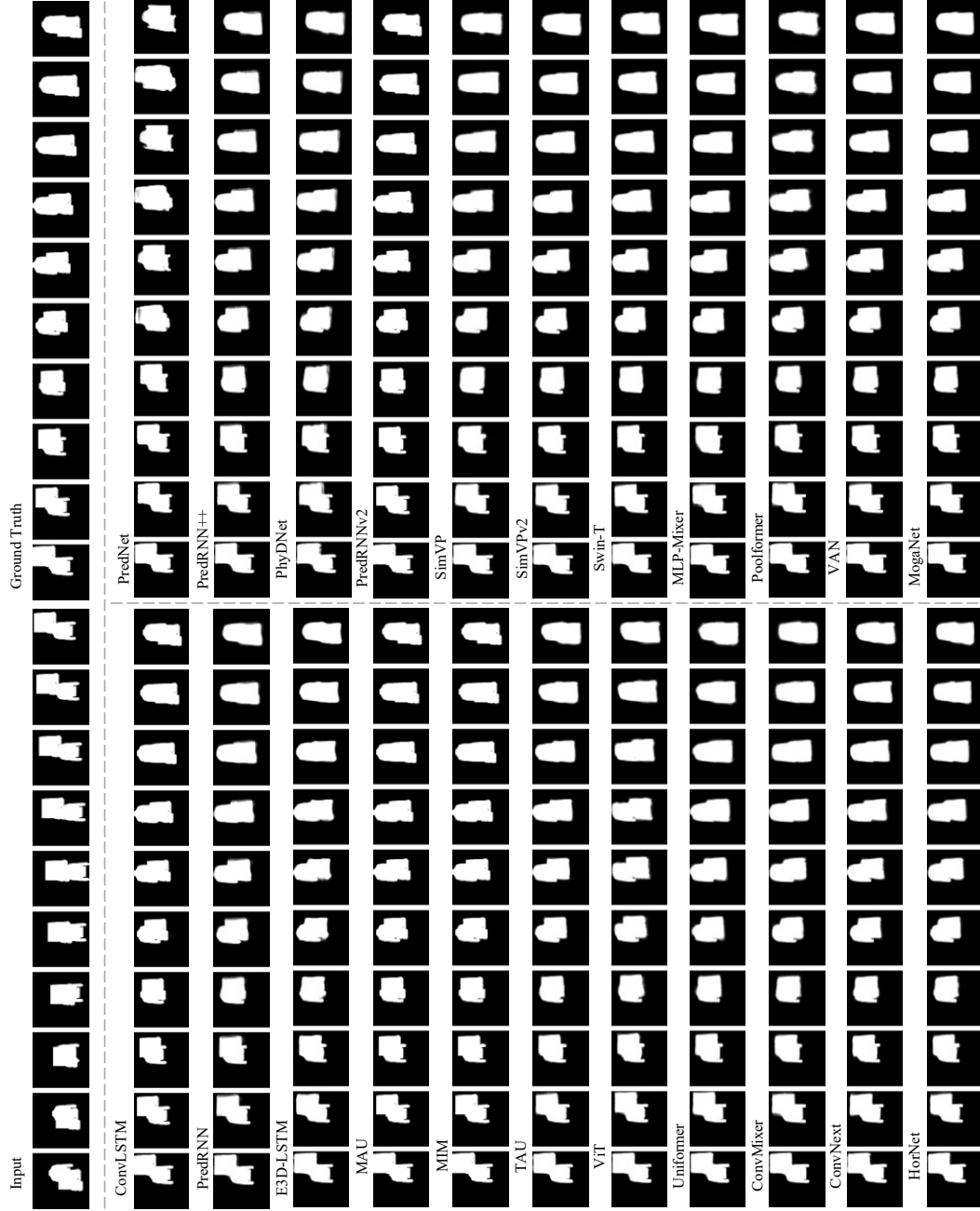


Figure 6: The qualitative visualization on Moving Fashion MNIST. For the convenience of formatting, we arrange the frames vertically from bottom to top.

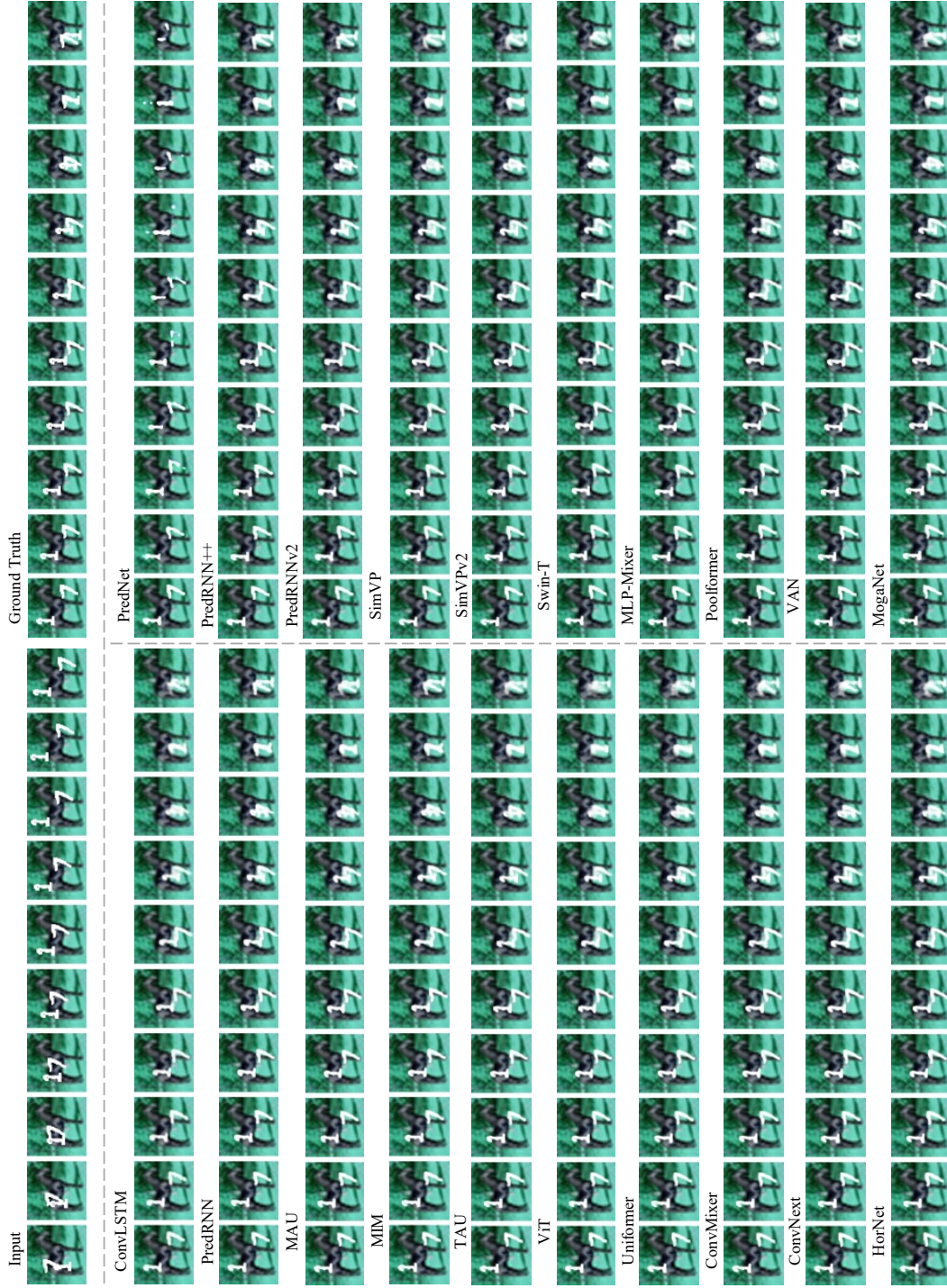


Figure 7: The qualitative visualization on Moving MNIST-CIFAR. For the convenience of formatting, we arrange the frames vertically from bottom to top.

## D.2 Real-world Video Prediction

**Kitties&Caltech** In addition to the quantitative results presented in the main text, we also provide a visualization example for qualitative assessment, as depicted in Figure 8. Interestingly, even though PredNet and DMVFN, which have limited temporal modeling capabilities, can still perform reasonably well in predicting the next frame.



Figure 8: The qualitative visualization on Kitti&Caltech.

**KTH** We showcase the quantitative results and qualitative visualization on KTH in Table 8 and Figure 9, respectively. Recurrent-free models demonstrate comparable performance while requiring few computational costs, thus striking a favorable balance between performance and efficiency.

Table 8: The performance on the KTH dataset.

	Method	Params (M)	FLOPs (G)	FPS	MSE ↓	MAE ↓	SSIM ↑	PSNR ↑	LPIPS ↓
Recurrent-based	ConvLSTM	14.9	1368.0	16	47.65	445.50	0.8977	26.99	0.26686
	PredNet	12.5	3.4	399	152.11	783.10	0.8094	22.45	0.32159
	PredRNN	23.6	2800.0	7	41.07	380.60	0.9097	27.95	0.21892
	PredRNN++	38.3	4162.0	5	<b>39.84</b>	<b>370.40</b>	<b>0.9124</b>	<b>28.13</b>	0.19871
	MIM	39.8	1099.0	17	40.73	380.80	0.9025	27.78	0.18808
	E3D-LSTM	53.5	217.0	17	136.40	892.70	0.8153	21.78	0.48358
	PhyDNet	3.1	93.6	58	91.12	765.60	0.8322	23.41	0.50155
	MAU	20.1	399.0	8	51.02	471.20	0.8945	26.73	0.25442
	PredRNNv2	23.6	2815.0	7	39.57	368.80	0.9099	28.01	0.21478
	DMVFN	3.5	0.9	727	59.61	413.20	0.8976	26.65	<b>0.12842</b>
Recurrent-free	SimVP	12.2	62.8	77	41.11	397.10	0.9065	27.46	0.26496
	TAU	15.0	73.8	55	45.32	421.70	0.9086	27.10	0.22856
	SimVPv2	15.6	76.8	53	45.02	417.80	0.9049	27.04	0.25240
	ViT	12.7	112.0	28	56.57	459.30	0.8947	26.19	0.27494
	Swin-T	15.3	75.9	65	45.72	405.70	0.9039	27.01	0.25178
	Uniformer	11.8	78.3	43	44.71	404.60	0.9058	27.16	0.24174
	MLP-Mixer	20.3	66.6	34	57.74	517.40	0.8886	25.72	0.28799
	ConvMixer	1.5	18.3	175	47.31	446.10	0.8993	26.66	0.28149
	Poolformer	12.4	63.6	67	45.44	400.90	0.9065	27.22	0.24763
	ConvNext	12.5	63.9	72	45.48	428.30	0.9037	26.96	0.26253
	VAN	14.9	73.8	55	45.05	409.10	0.9074	27.07	0.23116
	HorNet	15.3	75.3	58	46.84	421.20	0.9005	26.80	0.26921
	MogaNet	15.6	76.7	48	42.98	418.70	0.9065	27.16	0.25146

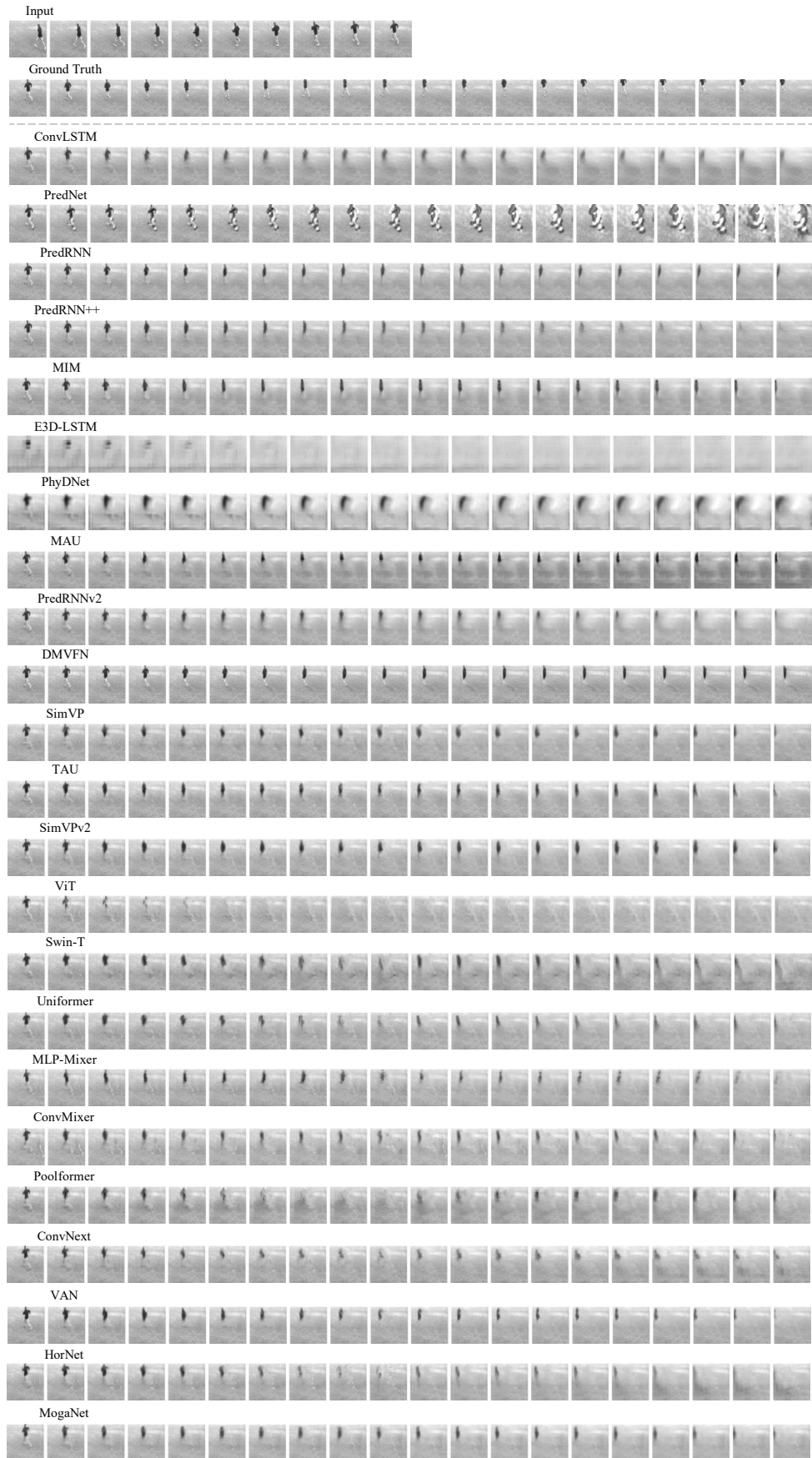


Figure 9: The qualitative visualization on KTH.



**Human3.6M** The quantitative results are presented in Table 9, and the qualitative visualization is depicted in Figure 10. In this task, human motion exhibits subtle changes between adjacent frames, resulting in a low-frequency signal of overall dynamics. Consequently, recurrent-free models, which excel at spatial learning, can efficiently and accurately predict future frames.

Table 9: The performance on the Human3.6M dataset.

	Method	Params (M)	FLOPs (G)	FPS	MSE ↓	MAE ↓	SSIM ↑	PSNR ↑	LPIPS ↓
Recurrent-based	ConvLSTM	15.5	347.0	52	125.5	1566.7	0.9813	33.40	0.03557
	PredNet	12.5	13.7	176	261.9	1625.3	0.9786	31.76	0.03264
	PredRNN	24.6	704.0	25	113.2	1458.3	0.9831	33.94	0.03245
	PredRNN++	39.3	1033.0	18	110.0	1452.2	0.9832	34.02	0.03196
	MIM	47.6	1051.0	17	112.1	1467.1	0.9829	33.97	0.03338
	E3D-LSTM	60.9	542.0	7	143.3	1442.5	0.9803	32.52	0.04133
	PhyDNet	4.2	19.1	57	125.7	1614.7	0.9804	33.05	0.03709
	MAU	20.2	105.0	6	127.3	1577.0	0.9812	33.33	0.03561
	PredRNNv2	24.6	708.0	24	114.9	1484.7	0.9827	33.84	0.03334
Recurrent-free	DMVFN	8.6	63.6	341	109.3	1449.3	0.9833	34.05	0.03189
	SimVP	41.2	197.0	26	115.8	1511.5	0.9822	33.73	0.03467
	TAU	37.6	182.0	26	113.3	<b>1390.7</b>	<b>0.9839</b>	34.03	<b>0.02783</b>
	SimVPv2	11.3	74.6	52	108.4	1441.0	0.9834	<b>34.08</b>	0.03224
	ViT	28.3	239.0	17	136.3	1603.5	0.9796	33.10	0.03729
	Swin	38.8	188.0	28	133.2	1599.7	0.9799	33.16	0.03766
	Uniformer	27.7	211.0	14	116.3	1497.7	0.9824	33.76	0.03385
	MLP-Mixer	47.0	164.0	34	125.7	1511.9	0.9819	33.49	0.03417
	ConvMixer	3.1	39.4	84	115.8	1527.4	0.9822	33.67	0.03436
	Poolformer	31.2	156.0	30	118.4	1484.1	0.9827	33.78	0.03313
	ConvNext	31.4	157.0	33	113.4	1469.7	0.9828	33.86	0.03305
	VAN	37.5	182.0	24	111.4	1454.5	0.9831	33.93	0.03335
	HorNet	28.1	143.0	33	118.1	1481.1	0.9825	33.73	0.03333
	MogaNet	8.6	163.6	56	109.1	1446.4	0.9834	34.05	0.03163

### D.3 Traffic and Weather Forecasting

#### D.3.1 TaxiBJ

We show the quantitative results in Table 10 and qualitative visualizations in Figure 11. The recurrent-free models have shown promising results in low-frequency traffic flow data than their counterparts.

Table 10: The performance on the TaxiBJ dataset.

	Method	Params (M)	FLOPs (G)	FPS	MSE ↓	MAE ↓	SSIM ↑
Recurrent-based	ConvLSTM	15.0	20.7	815	0.3358	15.32	0.9836
	PredNet	12.5	0.9	5031	0.3516	15.91	0.9828
	PredRNN	23.7	42.4	416	0.3194	15.31	0.9838
	PredRNN++	38.4	63.0	301	0.3348	15.37	0.9834
	MIM	37.9	64.1	275	0.3110	14.96	0.9847
	E3DLSTM	51.0	98.19	60	0.3421	14.98	0.9842
	PhyDNet	3.1	5.6	982	0.3622	15.53	0.9828
	MAU	4.4	6.0	540	0.3268	15.26	0.9834
	PredRNNv2	23.7	42.6	378	0.3834	15.55	0.9826
Recurrent-free	DMVFN	3.5	57.1	4772	0.3517	15.72	0.9833
	SimVP	13.8	3.6	533	0.3282	15.45	0.9835
	TAU	9.6	2.5	1268	0.3108	14.93	<b>0.9848</b>
	SimVPv2	10.0	2.6	1217	0.3246	15.03	0.9844
	ViT	9.7	2.8	1301	0.3171	15.15	0.9841
	Swin Transformer	9.7	2.6	1506	0.3128	15.07	0.9847
	Uniformer	9.5	2.7	1333	0.3268	15.16	0.9844
	MLP-Mixer	8.2	2.2	1974	0.3206	15.37	0.9841
	ConvMixer	0.8	0.2	4793	0.3634	15.63	0.9831
	Poolformer	7.6	2.1	1827	0.3273	15.39	0.9840
	ConvNext	7.8	2.1	1918	<b>0.3106</b>	<b>14.90</b>	0.9845
	VAN	9.5	2.5	1273	0.3125	14.96	<b>0.9848</b>
	HorNet	9.7	2.5	1350	0.3186	15.01	0.9843
	MogaNet	10.0	2.6	1005	0.3114	15.06	0.9847

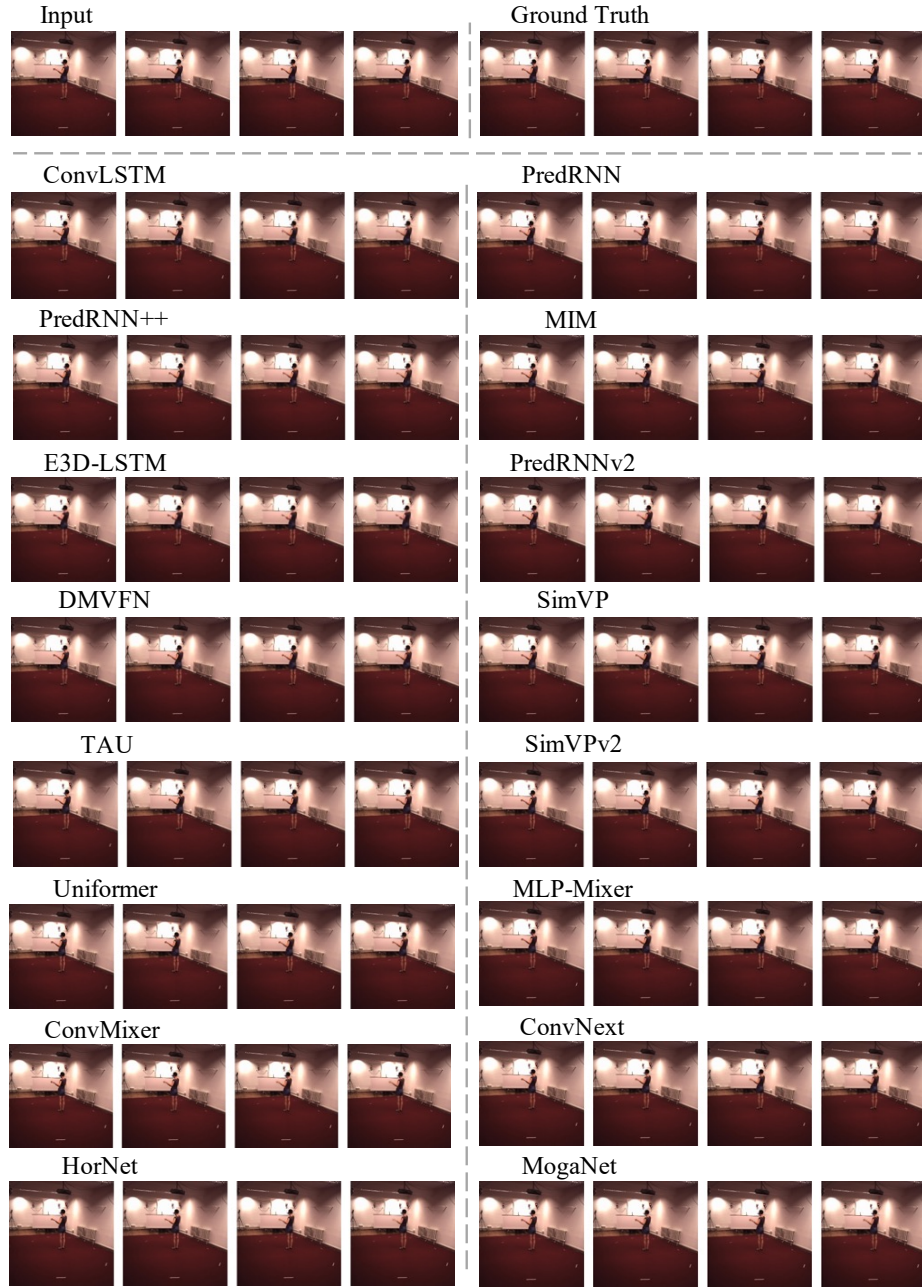
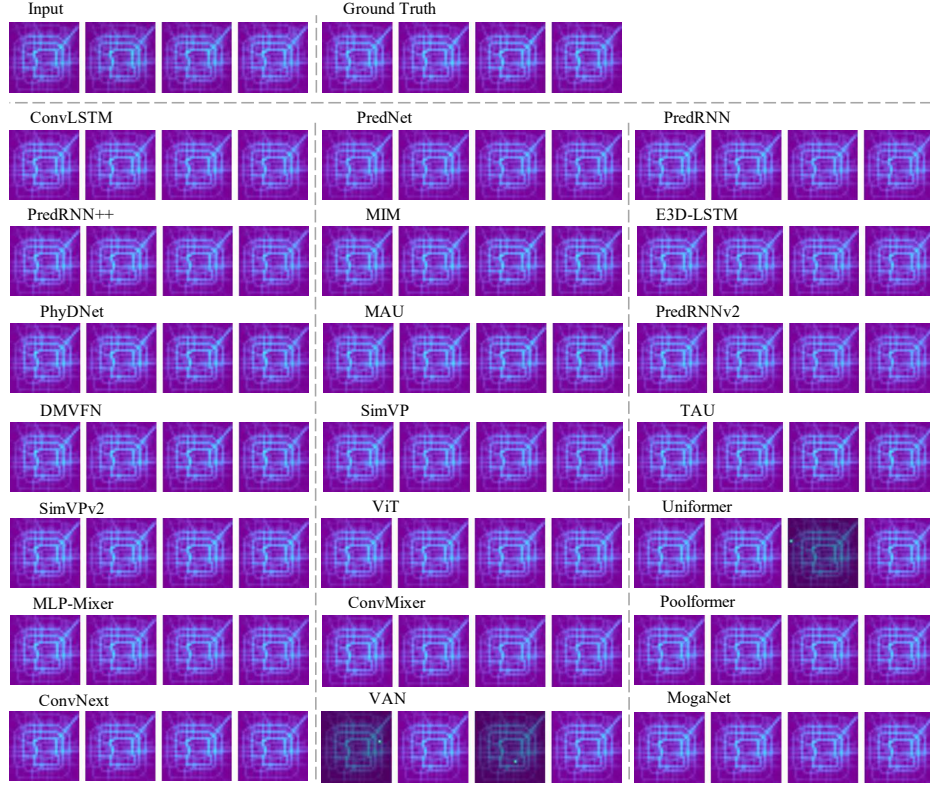
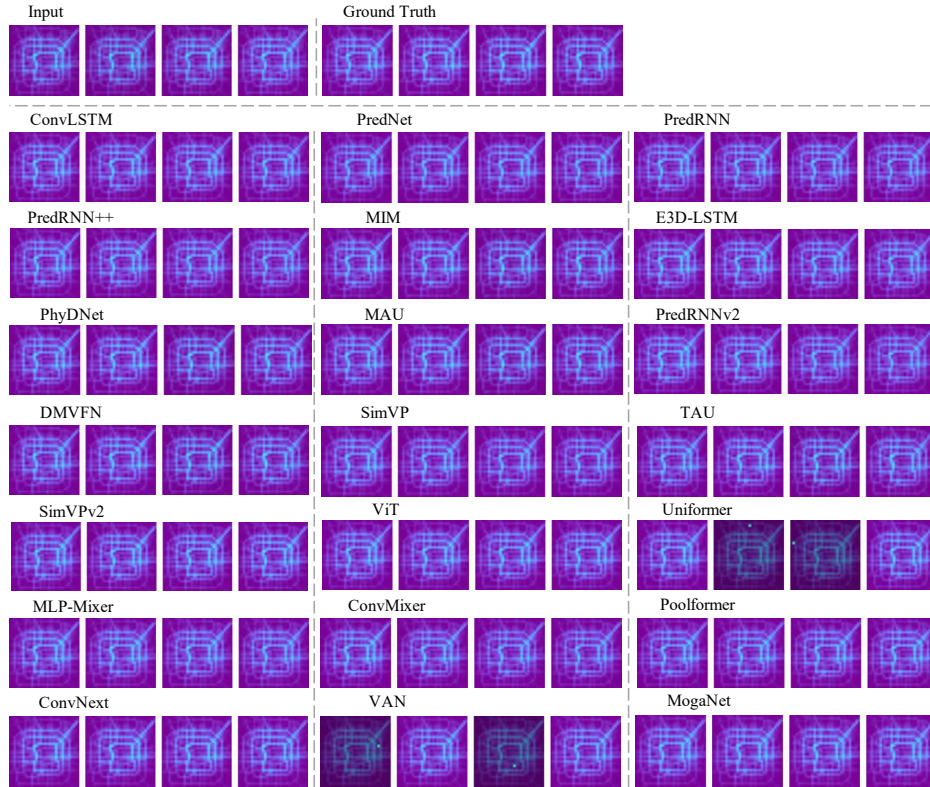


Figure 10: The qualitative visualization on Human3.6M.





(a) InFlow of TaxBJ



(b) OutFlow of TaxBJ

Figure 11: The qualitative visualization on TaxiBJ.

### D.3.2 WeatherBench

We strongly recommend readers refer to the GIF animations provided in our GitHub ([OpenSTL/docs/en/visualization/](https://github.com/OpenSTL/docs/en/visualization/)), as they provide a clearer visualization of the model’s prediction performance.

**Single-variable Temperature Forecasting** The quantitative results and qualitative visualization are presented in Table 11 and Figure 12. The recurrent-free models exhibit a clear superiority over the recurrent-based models in terms of both performance and efficiency, achieving a landslide victory.

Table 11: The performance on the single-variable temperature forecasting in WeatherBench.

	Method	Params (M)	FLOPs (G)	FPS	MSE ↓	MAE ↓	RMSE ↓
Recurrent-based	ConvLSTM	14.9	136.0	46	1.521	0.7949	1.233
	PredRNN	23.6	278.0	22	1.331	0.7246	1.154
	PredRNN++	38.3	413.0	15	1.634	0.7883	1.278
	MIM	37.8	109.0	126	1.784	0.8716	1.336
	PhyDNet	3.1	36.8	177	285.9	8.7370	16.91
	MAU	5.5	39.6	237	1.251	0.7036	1.119
	PredRNNv2	23.6	279.0	22	1.545	0.7986	1.243
Recurrent-free	SimVP	14.7	8.0	160	1.238	0.7037	1.113
	TAU	12.2	6.7	511	1.162	0.6707	1.078
	SimVPv2	12.8	7.0	504	<b>1.105</b>	<b>0.6567</b>	<b>1.051</b>
	ViT	12.4	8.0	432	1.146	0.6712	1.070
	Swin Transformer	12.4	6.9	581	1.143	0.6735	1.069
	Uniformer	12.0	7.5	465	1.204	0.6885	1.097
	MLP-Mixer	11.1	5.9	713	1.255	0.7011	1.119
	ConvMixer	1.1	1.0	1705	1.267	0.7073	1.126
	Poolformer	10.0	5.6	722	1.156	0.6715	1.075
	ConvNext	10.1	5.7	689	1.277	0.7220	1.130
	VAN	12.2	6.7	523	1.150	0.6803	1.072
	HorNet	12.4	6.8	517	1.201	0.6906	1.096
	MogaNet	12.8	7.0	416	1.152	0.6665	1.073

**Single-variable Humidity Forecasting** The quantitative results and qualitative visualization are presented in Table 12 and Figure 13. The results are almost consistent with the temperature forecasting.

Table 12: The performance on the single-variable humidity forecasting in WeatherBench.

	Method	Params (M)	FLOPs (G)	FPS	MSE ↓	MAE ↓	RMSE ↓
Recurrent-based	ConvLSTM	14.9	136.0	46	35.146	4.012	5.928
	PredRNN	23.6	278.0	22	37.611	4.096	6.133
	PredRNN++	38.3	413.0	15	45.993	4.731	6.782
	MIM	37.8	109.0	126	61.113	5.504	7.817
	PhyDNet	3.1	36.8	177	239.0	8.975	15.46
	MAU	5.5	39.6	237	34.529	4.004	5.876
	PredRNNv2	23.6	279.0	22	36.508	4.087	6.042
Recurrent-free	SimVP	14.7	8.0	160	34.355	3.994	5.861
	TAU	12.2	6.7	511	31.831	3.818	5.642
	SimVPv2	12.8	7.0	504	31.426	<b>3.765</b>	5.606
	ViT	12.4	8.0	432	32.616	3.852	5.711
	Swin Transformer	12.4	6.9	581	<b>31.332</b>	3.776	<b>5.597</b>
	Uniformer	12.0	7.5	465	32.199	3.864	5.674
	MLP-Mixer	11.1	5.9	713	34.467	3.950	5.871
	ConvMixer	1.1	1.0	1705	32.829	3.909	5.730
	Poolformer	10.0	5.6	722	31.989	3.803	5.656
	ConvNext	10.1	5.7	689	33.179	3.928	5.760
	VAN	12.2	6.7	523	31.712	3.812	5.631
	HorNet	12.4	6.8	517	32.081	3.826	5.664
	MogaNet	12.8	7.0	416	31.795	3.816	5.639



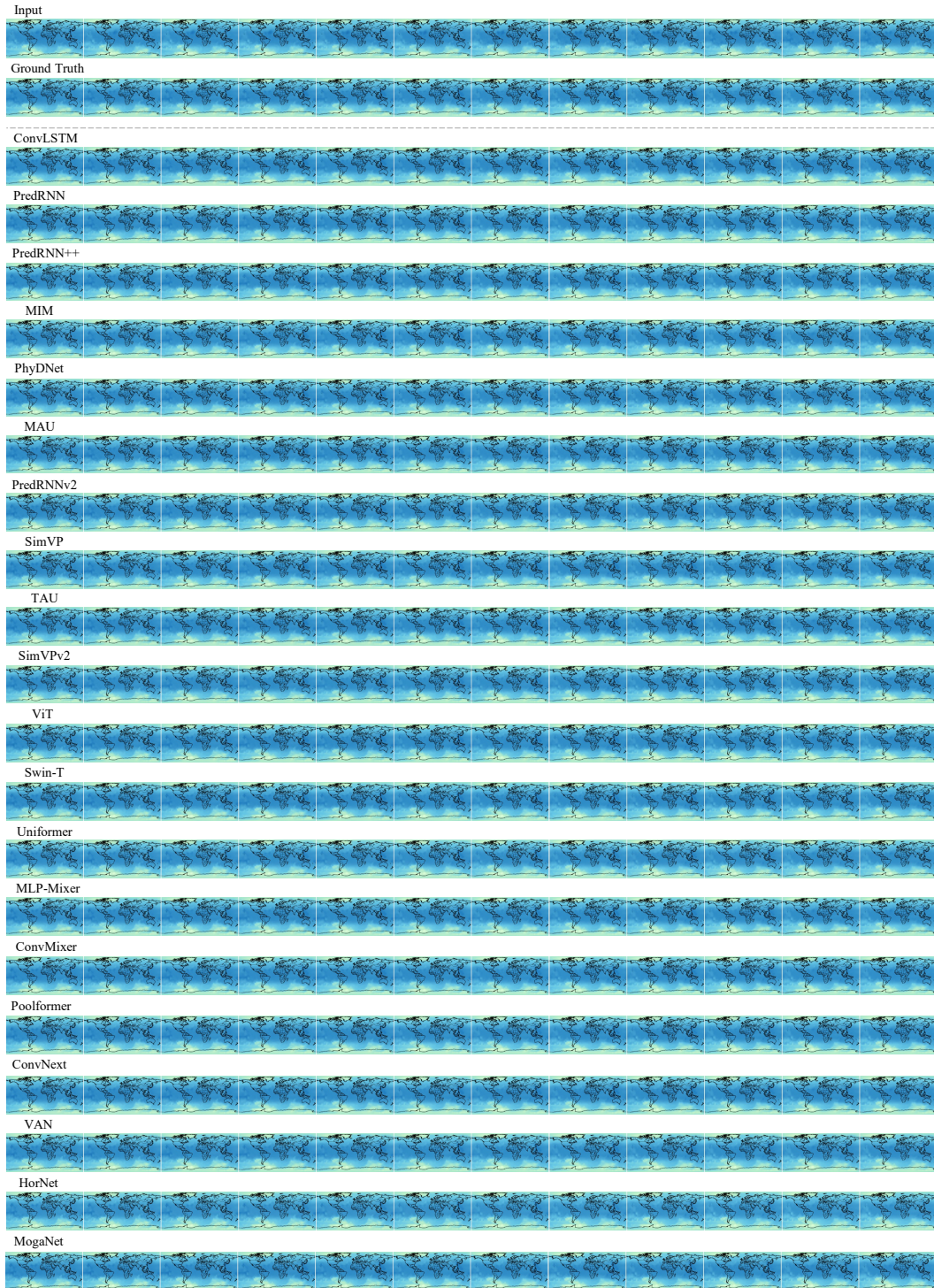


Figure 12: The qualitative visualization on the single-variable temperature forecasting in the Weather-Bench dataset.



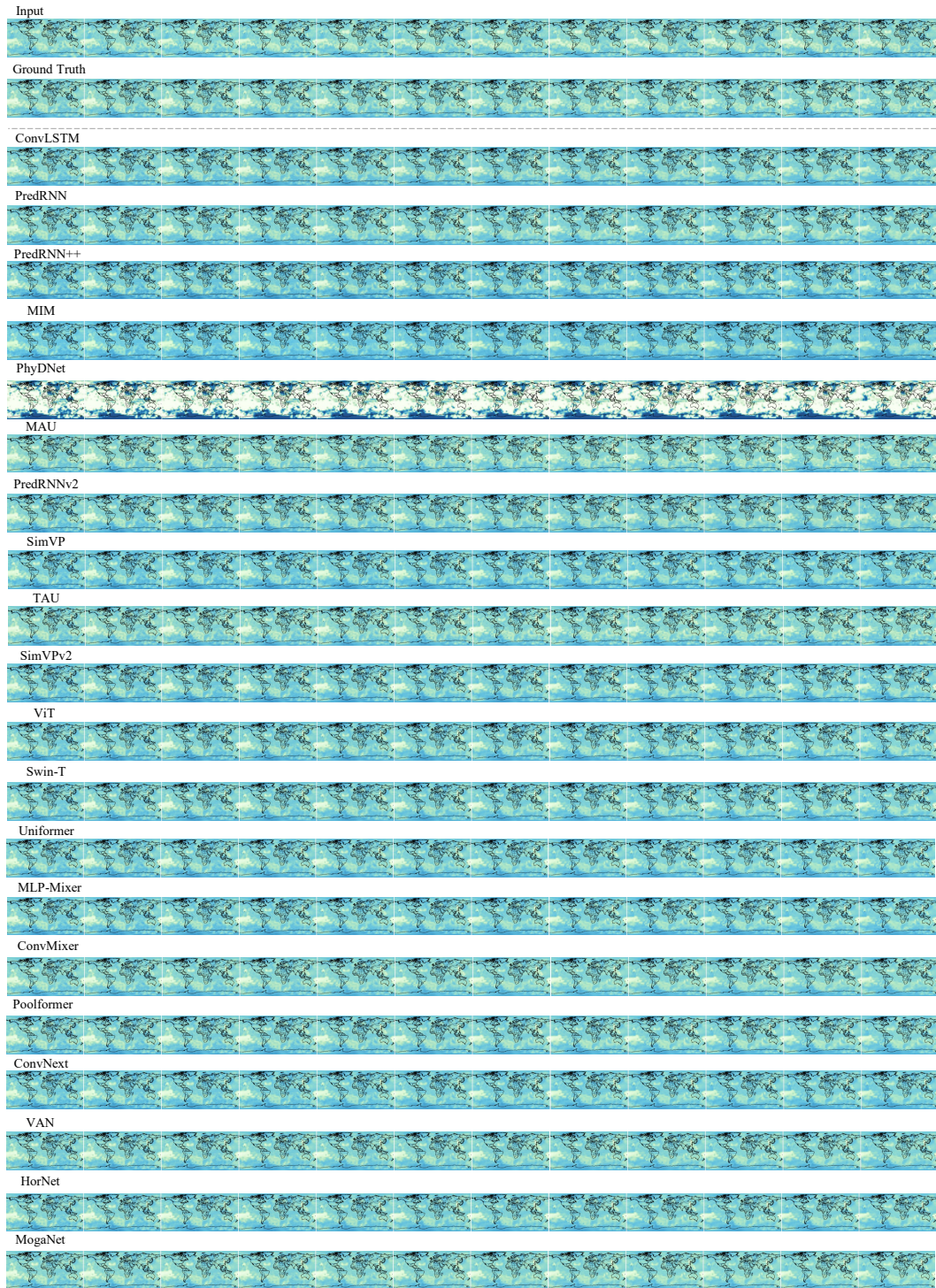


Figure 13: The qualitative visualization on the single-variable humidity forecasting in the Weather-Bench dataset.

**Single-variable Wind Component Forecasting** The quantitative results are presented in Table 13. The qualitative visualizations of latitude and longitude wind are shown in Figure 14 and Figure 15. Most recurrent-free models outperform the recurrent-based models.

Table 13: The performance on the single-variable wind component forecasting in WeatherBench.

	Method	Params (M)	FLOPs (G)	FPS	MSE ↓	MAE ↓	RMSE ↓
Recurrent-based	ConvLSTM	15.0	136.0	43	1.8976	0.9215	1.3775
	PredRNN	23.7	279.0	21	1.8810	0.9068	1.3715
	PredRNN++	38.4	414.0	14	1.8727	0.9019	1.3685
	MIM	37.8	109.0	122	3.1399	1.1837	1.7720
	PhyDNet	3.1	36.8	172	16.7983	2.9208	4.0986
	MAU	5.5	39.6	233	1.9001	0.9194	1.3784
	PredRNNv2	23.7	280.0	21	2.0072	0.9413	1.4168
Recurrent-free	SimVP	14.7	8.0	430	1.9993	0.9510	1.4140
	TAU	12.2	6.7	505	1.5925	0.8426	1.2619
	SimVPv2	12.8	7.0	529	1.5069	0.8142	1.2276
	ViT	12.4	8.0	427	1.6262	0.8438	1.2752
	Swin Transformer	12.4	6.9	559	<b>1.4996</b>	0.8145	<b>1.2246</b>
	Uniformer	12.0	7.5	466	1.4850	<b>0.8085</b>	1.2186
	MLP-Mixer	11.1	5.9	687	1.6066	0.8395	1.2675
	ConvMixer	1.1	1.0	1807	1.7067	0.8714	1.3064
	Poolformer	10.0	5.6	746	1.6123	0.8410	1.2698
	ConvNext	10.1	5.7	720	1.6914	0.8698	1.3006
	VAN	12.2	6.7	549	1.5958	0.8371	1.2632
	HorNet	12.4	6.9	539	1.5539	0.8254	1.2466
	MogaNet	12.8	7.0	441	1.6072	0.8451	1.2678

**Single-variable Cloud Cover Forecasting** The quantitative results and visualization are presented in Table 14 and Figure 16. All the recurrent-free models perform better than their counterparts.

Table 14: The performance on the single-variable cloud cover forecasting in WeatherBench.

	Method	Params (M)	FLOPs (G)	FPS	MSE ↓	MAE ↓	RMSE ↓
Recurrent-based	ConvLSTM	14.9	136.0	46	0.04944	0.15419	0.222
	PredRNN	23.6	278.0	22	0.05504	0.15877	0.234
	PredRNN++	38.3	413.0	15	0.05479	0.15435	0.234
	MIM	37.75	109.0	126	0.05997	0.17184	0.245
	PhyDNet	3.1	36.8	177	0.09913	0.22614	0.314
	MAU	5.5	39.6	237	0.04955	0.15158	0.222
	PredRNNv2	23.6	279.0	22	0.05051	0.15867	0.224
Recurrent-free	SimVP	14.7	8.0	160	0.04765	0.15029	0.218
	TAU	12.2	6.7	511	0.04723	<b>0.14604</b>	0.217
	SimVPv2	12.8	7.0	504	0.04657	0.14688	0.215
	ViT	12.4	8.0	432	0.04778	0.15026	0.218
	Swin Transformer	12.4	6.9	581	<b>0.04639</b>	0.14729	<b>0.215</b>
	Uniformer	12.0	7.5	465	0.04680	0.14777	0.216
	MLP-Mixer	11.1	5.9	713	0.04925	0.15264	0.221
	ConvMixer	1.1	1.0	1705	0.04717	0.14874	0.217
	Poolformer	10.0	5.6	722	0.04694	0.14884	0.216
	ConvNext	10.1	5.7	689	0.04742	0.14867	0.217
	VAN	12.2	6.7	523	0.04694	0.14725	0.216
	HorNet	12.4	6.8	517	0.04692	0.14751	0.216
	MogaNet	12.8	7.0	416	0.04699	0.14802	0.216



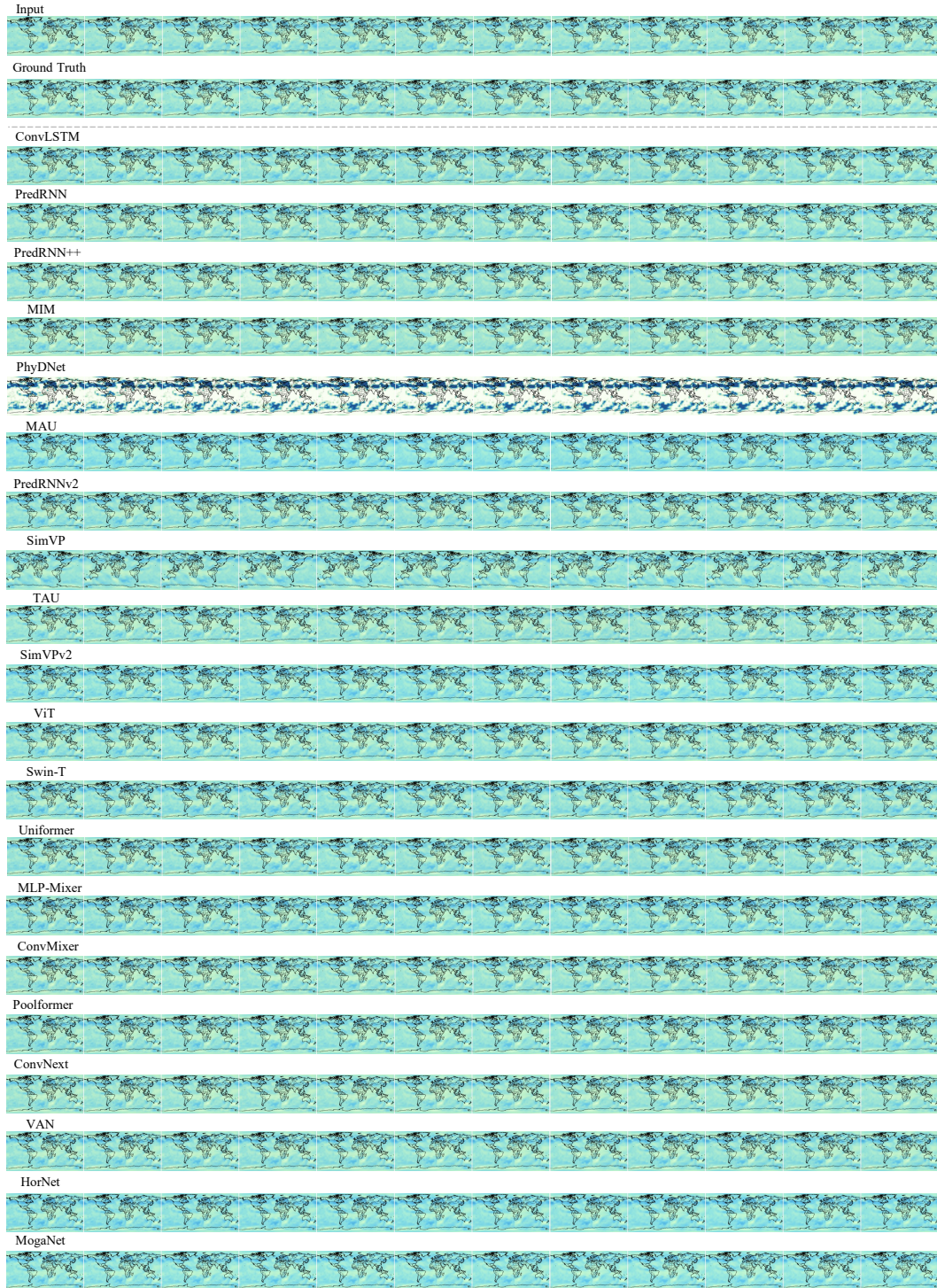


Figure 14: The qualitative visualization on the single-variable latitude wind forecasting in the WeatherBench dataset.



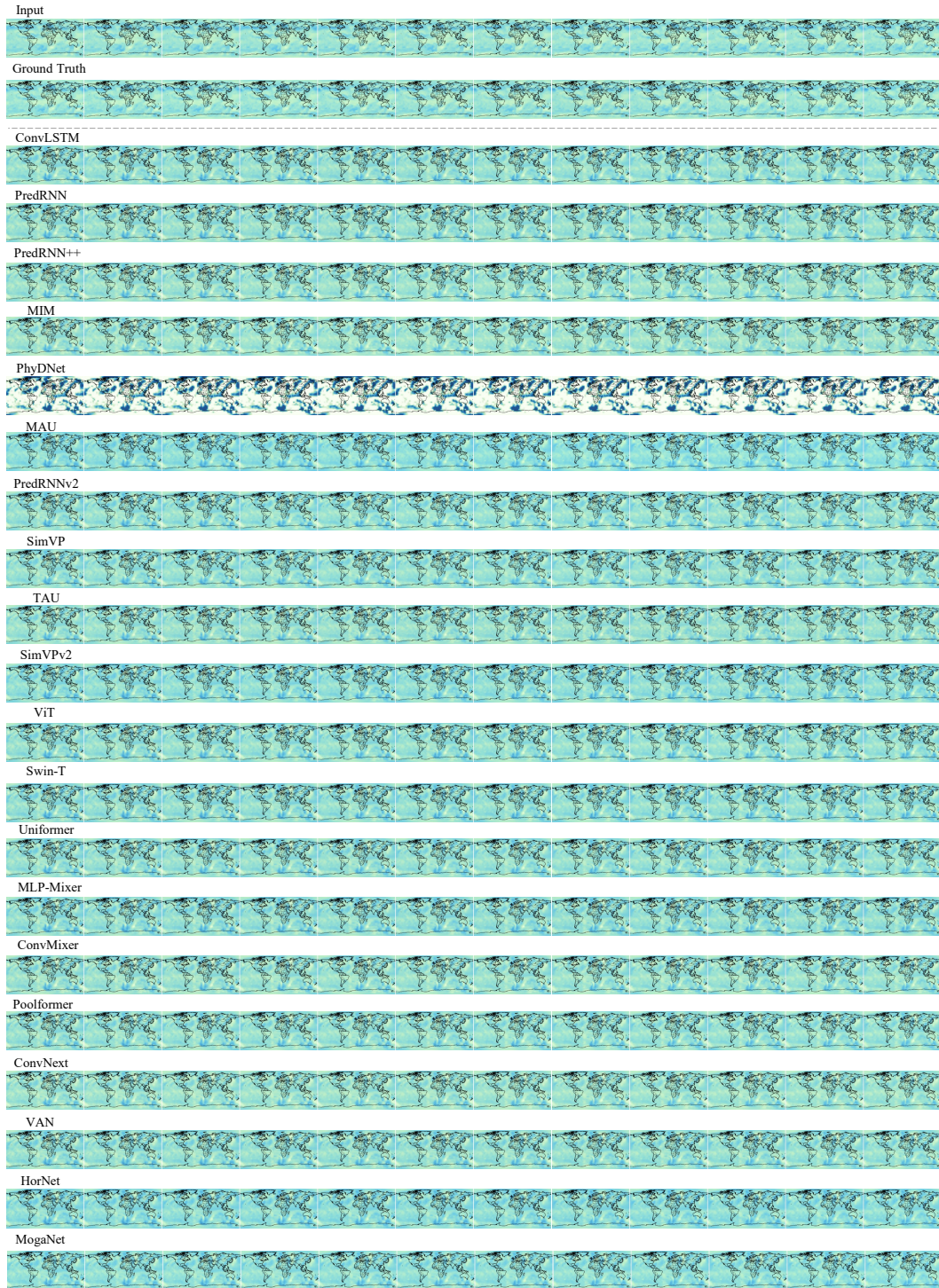


Figure 15: The qualitative visualization on the single-variable longitude wind forecasting in the WeatherBench dataset.



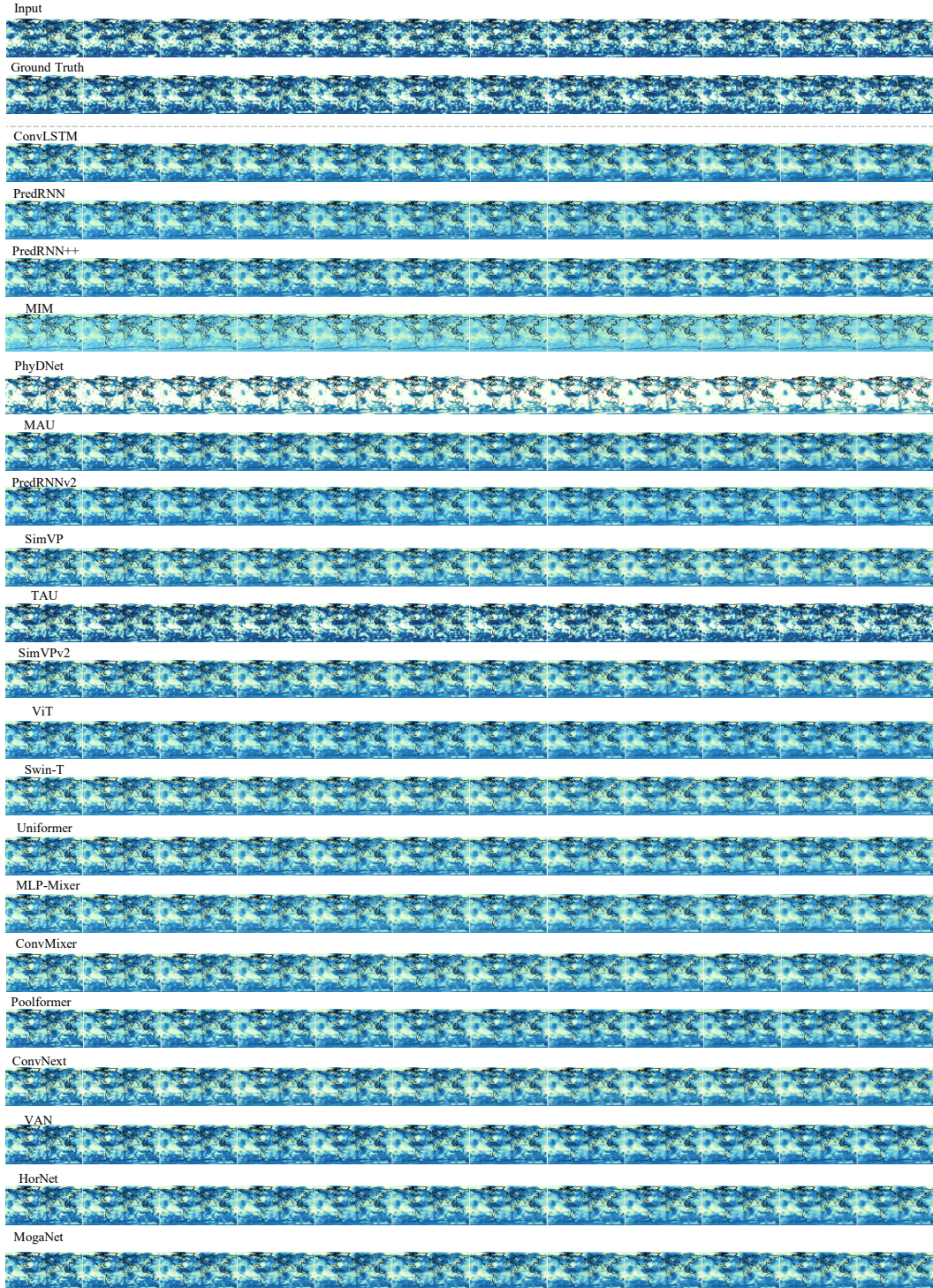


Figure 16: The qualitative visualization on the single-variable cloud cover forecasting in the Weather-Bench dataset.

**Single-variable Temperature Forecasting with High Resolution** We perform experiments on high-resolution ( $128 \times 256$ ) temperature forecasting. The quantitative results are presented in Table 15. SimVPv2 achieves remarkable performance, surpassing the recurrent-based models by large margins.

Table 15: The performance on the single-variable high-resolution ( $128 \times 256$ ) temperature forecasting.

Method	Params (M)	FLOPs (G)	FPS	MSE ↓	MAE ↓	RMSE ↓
Recurrent-based	ConvLSTM	15.0	550.0	35	1.0625	0.6517
	PredRNN	23.8	1123.0	3	0.8966	0.5869
	PredRNN++	38.6	1663.0	2	0.8538	0.5708
	MIM	42.2	1739.0	11	1.2138	0.6857
	PhyDNet	3.1	148.0	41	297.34	8.9788
	MAU	11.8	172.0	17	1.0031	0.6316
	PredRNNv2	23.9	1129.0	3	1.0451	0.6190
Recurrent-free	SimVP	14.7	128.0	27	0.8492	0.5636
	TAU	12.3	36.1	94	0.8316	0.5615
	SimVPv2	12.8	112.0	33	<b>0.6499</b>	<b>0.4909</b>
	ViT	12.5	36.8	50	0.8969	0.5834
	Swin Transformer	12.4	110.0	38	0.7606	0.5193
	Uniformer	12.1	48.8	57	1.0052	0.6294
	MLP-Mixer	27.9	94.7	49	1.1865	0.6593
	ConvMixer	1.1	15.1	117	0.8557	0.5669
	Poolformer	10.0	89.7	42	0.7983	0.5316
	ConvNext	10.1	90.5	47	0.8058	0.5406
	VAN	12.2	107.0	34	0.7110	0.5094
	HorNet	12.4	109.0	34	0.8250	0.5467
	MogaNet	12.8	112.0	27	0.7517	0.5232

**Multiple-variable Forecasting** This task focuses on multi-factor climate prediction. We include temperature, humidity, latitude wind, and longitude factors in the forecasting process. The comprehensive results can be found in Table 16 to Table 19. We also show a comparison in Figure 17. MogaNet achieves significant leading performance across various metrics in predicting climatic factors.

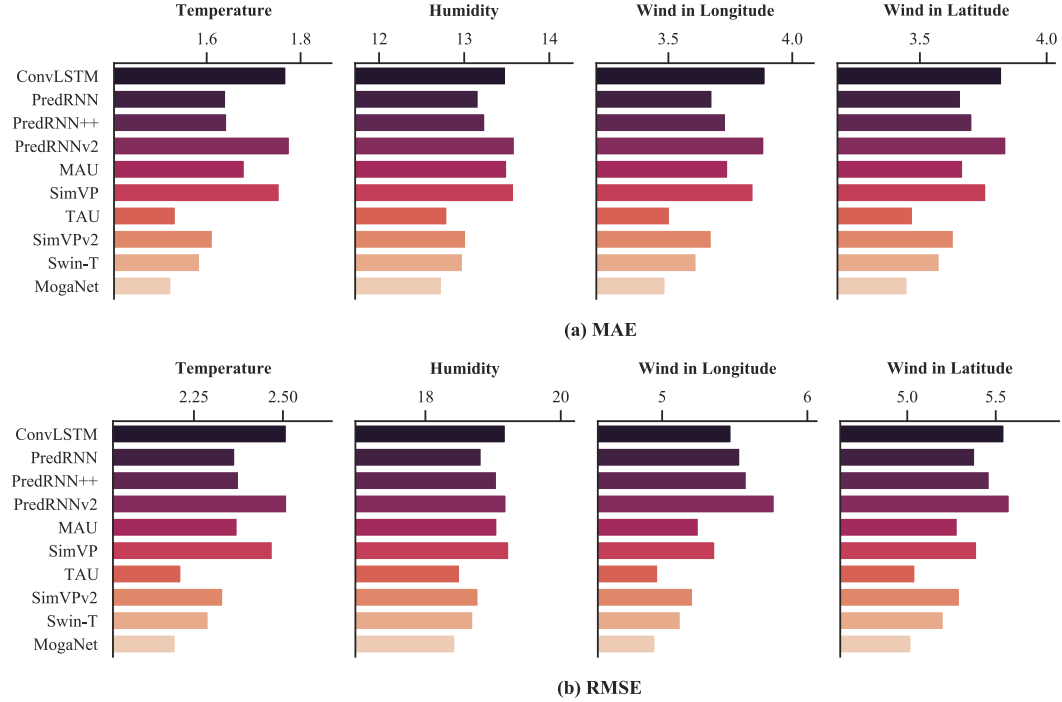


Figure 17: The (a) MAE and (b) RMSE metrics of the representative approaches on the four weather forecasting tasks in WeatherBench (Muti-variable setting).

Table 16: The performance on the multiple-variable temperature forecasting in WeatherBench.

	Method	Params (M)	FLOPs (G)	MSE ↓	MAE ↓	RMSE ↓
Recurrent-based	ConvLSTM	15.5	43.3	6.3034	1.7695	2.5107
	PredRNN	24.6	88.0	5.5966	1.6411	2.3657
	PredRNN++	39.3	129.0	5.6471	1.6433	2.3763
	MIM	5.5	12.1	7.5152	1.9650	2.7414
	PhyDNet	3.1	11.3	95.113	6.4749	9.7526
	MAU	5.5	12.1	5.6287	1.6810	2.3725
	PredRNNv2	24.6	88.5	6.3078	1.7770	2.5115
Recurrent-free	SimVP	13.8	7.3	6.1068	1.7554	2.4712
	TAU	9.6	5.0	4.9042	1.5341	2.2145
	SimVPv2	10.0	5.3	5.4382	1.6129	2.3319
	ViT	9.7	6.1	5.2722	1.6005	2.2961
	Swin Transformer	9.7	5.2	5.2486	1.5856	2.2910
	Unifomer	9.5	5.9	5.1174	1.5758	2.2622
	MLP-Mixer	8.7	4.4	5.8546	1.6948	2.4196
	ConvMixer	0.9	0.5	6.5838	1.8228	2.5659
	Poolformer	7.8	4.1	7.1077	1.8791	2.6660
	ConvNext	7.9	4.2	6.1749	1.7448	2.4849
	VAN	9.5	5.0	4.9396	1.5390	2.2225
	HorNet	9.7	5.1	5.5856	1.6198	2.3634
	MogaNet	10.0	5.3	<b>4.8335</b>	<b>1.5246</b>	<b>2.1985</b>

Table 17: The performance on the multiple-variable humidity forecasting in WeatherBench.

	Method	Params (M)	FLOPs (G)	MSE ↓	MAE ↓	RMSE ↓
Recurrent-based	ConvLSTM	15.5	43.3	368.15	13.490	19.187
	PredRNN	24.6	88.0	354.57	13.169	18.830
	PredRNN++	39.3	129.0	363.15	13.246	19.056
	MIM	41.7	35.8	408.24	14.658	20.205
	PhyDNet	3.1	11.3	668.40	21.398	25.853
	MAU	5.5	12.1	363.36	13.503	19.062
	PredRNNv2	24.6	88.5	368.52	13.594	19.197
Recurrent-free	SimVP	13.8	7.3	370.03	13.584	19.236
	TAU	9.6	5.0	342.63	12.801	<b>18.510</b>
	SimVPv2	10.0	5.3	352.79	13.021	18.783
	ViT	9.7	6.1	352.36	13.056	18.771
	Swin Transformer	9.7	5.2	349.92	<b>12.984</b>	18.706
	Unifomer	9.5	5.9	351.66	12.994	18.753
	MLP-Mixer	8.7	4.4	365.48	13.408	19.118
	ConvMixer	0.9	0.5	381.85	13.917	19.541
	Poolformer	7.8	4.1	380.18	13.908	19.498
	ConvNext	7.9	4.2	367.39	13.516	19.168
	VAN	9.5	5.0	343.61	12.790	18.537
	HorNet	9.7	5.1	353.02	13.024	18.789
	MogaNet	10.0	5.3	<b>340.06</b>	12.738	18.441

Table 18: The performance on the multiple-variable latitude wind forecasting in WeatherBench.

	Method	Params (M)	FLOPs (G)	MSE ↓	MAE ↓	RMSE ↓
Recurrent-based	ConvLSTM	15.5	43.3	30.789	3.8238	5.5488
	PredRNN	24.6	88.0	28.973	3.6617	5.3827
	PredRNN++	39.3	129.0	29.872	3.7067	5.4655
	MIM	41.7	35.8	36.464	4.2066	6.0386
	PhyDNet	3.1	11.3	54.389	5.1996	7.3749
	MAU	5.5	12.1	27.929	3.6700	5.2848
	PredRNNv2	24.6	88.5	31.120	3.8406	5.5785
Recurrent-free	SimVP	13.8	7.3	29.094	3.7614	5.3939
	TAU	9.6	5.0	25.456	3.4723	5.0454
	SimVPv2	10.0	5.3	28.058	3.6335	5.2970
	ViT	9.66	6.12	27.381	3.6068	5.2327
	Swin Transformer	9.7	5.2	27.097	3.5777	5.2055
	Uniformer	9.5	5.9	26.799	3.5676	5.1768
	MLP-Mixer	8.7	4.4	30.014	3.7840	5.4785
	ConvMixer	0.9	0.5	31.609	3.9104	5.6222
	Poolformer	7.8	4.1	35.161	4.0764	5.9296
	ConvNext	7.9	4.2	31.326	3.8435	5.5969
	VAN	9.5	5.0	25.720	3.4858	5.0715
	HorNet	9.7	5.1	30.028	3.7148	5.4798
	MogaNet	10.0	5.3	<b>25.232</b>	<b>3.4509</b>	<b>5.0231</b>

Table 19: The performance on the multiple-variable longitude wind forecasting in WeatherBench.

	Method	Params (M)	FLOPs (G)	MSE ↓	MAE ↓	RMSE ↓
Recurrent-based	ConvLSTM	15.5	43.3	30.002	3.8923	5.4774
	PredRNN	24.6	88.0	27.484	3.6776	5.2425
	PredRNN++	39.3	129.0	28.396	3.7322	5.3288
	MIM	41.7	35.8	35.586	4.2842	5.9654
	PhyDNet	3.1	11.3	97.424	7.3637	9.8704
	MAU	5.5	12.1	27.582	3.7409	5.2519
	PredRNNv2	24.6	88.5	29.833	3.8870	5.4620
Recurrent-free	SimVP	13.8	7.3	28.782	3.8435	5.3649
	TAU	9.6	5.0	24.719	3.5060	4.9719
	SimVPv2	10.0	5.3	27.166	3.6747	5.2121
	ViT	9.7	6.1	26.595	3.6472	5.1570
	Swin Transformer	9.7	5.2	26.292	3.6133	5.1276
	Uniformer	9.5	5.9	25.994	3.6069	5.0985
	MLP-Mixer	8.7	4.4	29.242	3.8407	5.4076
	ConvMixer	0.9	0.5	30.983	3.9949	5.5662
	Poolformer	7.8	4.1	33.757	4.1280	5.8101
	ConvNext	7.9	4.2	29.764	3.8688	5.4556
	VAN	9.5	5.0	24.991	3.5254	4.9991
	HorNet	9.7	5.1	28.192	3.7142	5.3096
	MogaNet	10.0	5.3	<b>24.535</b>	<b>3.4882</b>	<b>4.9533</b>